Dynamic chromatin accessibility tuning by the long noncoding RNA *ELDR* accelerates chondrocyte senescence and osteoarthritis

Graphical abstract

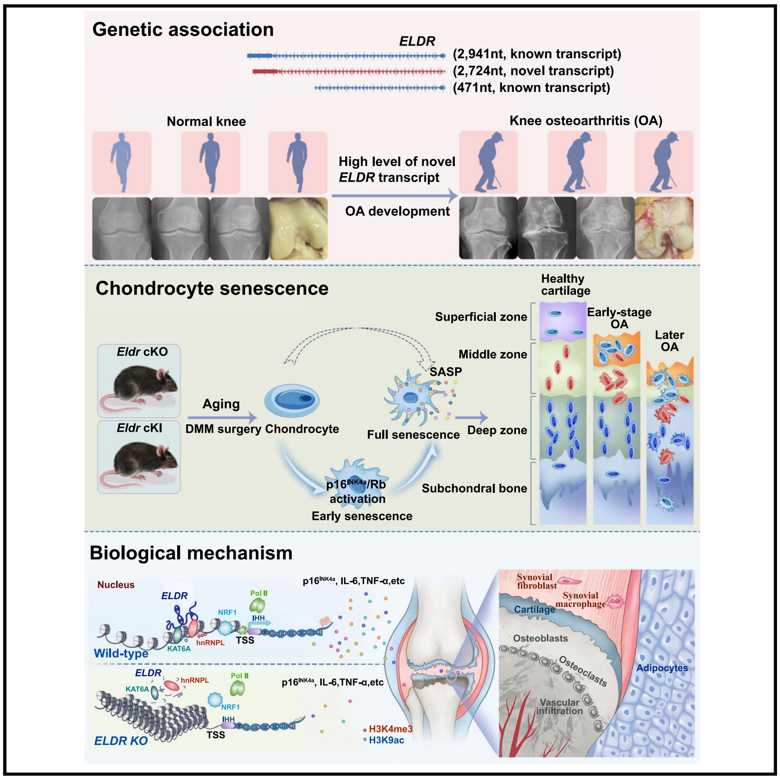

Authors

Ming-liang Ji, Zhuang Li, Xin Yue Hu, Wei tuo Zhang, Hai xiang Zhang, Jun Lu

Correspondence

jimingliang558@outlook.com (M.-l.J.),
junlusuper@outlook.com (J.L.)

Ji and colleagues identify *ELDR* as a critical regulator of chondrocyte senescence. Mechanistically, the core region of *ELDR* physically mediates a complex consisting of hnRNPL and KAT6A to regulate histone modifications of the promoter region of *IHH*, thereby activating hedgehog signaling.

Ji et al., 2023, The American Journal of Human Genetics *110*, 606–624
April 6, 2023
https://doi.org/10.1016/j.ajhg.2023.02.011

Dynamic chromatin accessibility tuning by the long noncoding RNA *ELDR* accelerates chondrocyte senescence and osteoarthritis

Ming-liang Ji,[1,*] Zhuang Li,[1] Xin Yue Hu,[1] Wei tuo Zhang,[1] Hai xiang Zhang,[1] and Jun Lu[1,*]

Summary

Epigenetic reprogramming plays a critical role in chondrocyte senescence during osteoarthritis (OA) pathology, but the underlying molecular mechanisms remain to be elucidated. Here, using large-scale individual datasets and genetically engineered (Col2a1-CreER^{T2};*Eldr*$^{flox/flox}$ and Col2a1-CreER^{T2};*ROSA26*-LSL-*Eldr*$^{+/+}$ knockin) mouse models, we show that a novel transcript of long noncoding RNA *ELDR* is essential for the development of chondrocyte senescence. *ELDR* is highly expressed in chondrocytes and cartilage tissues of OA. Mechanistically, exon 4 of *ELDR* physically mediates a complex consisting of hnRNPL and KAT6A to regulate histone modifications of the promoter region of *IHH*, thereby activating hedgehog signaling and promoting chondrocyte senescence. Therapeutically, GapmeR-mediated silencing of *ELDR* in the OA model substantially attenuates chondrocyte senescence and cartilage degradation. Clinically, *ELDR* knockdown in cartilage explants from OA-affected individuals decreased the expression of senescence markers and catabolic mediators. Taken together, these findings uncover an lncRNA-dependent epigenetic driver in chondrocyte senescence, highlighting that *ELDR* could be a promising therapeutic avenue for OA.

Introduction

Aging and trauma are crucial risk factors for the development of osteoarthritis (OA),[1–4] a highly prevalent and severely debilitating whole-joint disorder predominantly characterized by destruction of articular cartilage causing pain and functional disability.[5–8] Although the relationship between aging and OA is not fully understood, accumulating evidence suggests that aging-associated changes in articular tissues contribute to OA development.[3,4,9] From studies of surgically induced OA in young animals, osteoarthritic phenotypes in the joint can develop without a substantial contribution of aging, implying that aging and OA are inter-related but not inter-dependent.[3,10] Hence, a deeper understanding of how aging and trauma drive OA will undoubtedly enable the identification of a variety of potential therapeutic targets, which could have a major impact on public health.

In a physiological setting, the chondrocyte, the unique resident cell type in articular cartilage, maintains cartilage homeostasis via a delicate balance between anabolism and catabolism.[11,12] Under various pathological stimuli, chondrocytes undergo phenotypic shift, developing features of a senescent phenotype.[13,14] Mounting evidence indicates that chondrocyte senescence is potentially a common molecular mechanism that drives or promotes both age-associated and post-traumatic OA.[15,16] Senescent chondrocytes exhibit a variety of senescence-associated secretory phenotypes (SASPs).[15,16] Furthermore, several senescent cell (SnC) markers, including senescence-associated-galactosidase (SA-β-gal), levels of p16^{INK4A} (encoded by *CDKN2A*), and levels of p21 (encoded by *CDKN1A*) are found in osteoarthritic cartilage.[2] More intriguingly, clearance of SnCs decreased levels of senescent and inflammatory markers while also increasing levels of cartilage tissue extracellular matrix proteins, which implies that targeting SnCs might be an attractive therapeutic modality for treatment of OA.[2,17,18] However, the regulatory mechanisms underlying the senescent phenotypes of chondrocytes is not well characterized, and how these phenotypes can be controlled in OA cartilage remains poorly understood.

Long noncoding RNAs (lncRNAs) can bind DNA, RNA, or proteins to regulate cellular senescence.[4,19–21] For instance, the lncRNA *PANDA*, a p53-responsive lncRNA, is derived from the *CDKN1A* promoter and binds nuclear transcription factor Y subunit α (NF-YA) in senescent cells.[22] Concerning epigenetic regulation, the lncRNA *HOTAIR* is required to target polycomb repressive complex 2 (PRC2) occupancy and activity to silence transcription of the *HOXD* locus.[23] In addition, the lncRNA *Kcnq1ot1* interacts with chromatin and with the H3K9- and H3K27-specific histone modifications and the PRC2 complex in a lineage-specific manner in mice.[24] Similarly, silencing lncRNA-*OIS1* diminishes the senescent-associated induction of a nearby gene (dipeptidyl-peptidase 4, *DPP4*) with an established role in tumor suppression.[25] Also, lncRNA *UCA1* and CAPERα/TBX3 constitute a coordinated, reinforcing mechanism to regulate both *CDKN2A* transcription and mRNA stability, inducing senescence.[26] Notably, lncRNAs regulate target genes via triplex formation in *trans*.[27,28] lncRNAs have important functions in both development and diseases of the joints[29–31]; however, precise mechanisms of lncRNAs in chondrocyte senescence and cartilage degradation of OA have not yet been thoroughly investigated.

[1]The Center of Joint and Sports Medicine, Orthopedics Department, Zhongda Hospital, Southeast University, Nanjing, China
*Correspondence: jimingliang558@outlook.com (M.-l.J.), junlusuper@outlook.com (J.L.)
https://doi.org/10.1016/j.ajhg.2023.02.011.

Here, we identified a novel transcript of EGFR long non-coding downstream RNA (*ELDR*), which was markedly up-regulated in OA and significantly associated with cartilage degradation. The biological roles of *ELDR* in chondrocyte senescence and OA development were genetically assessed in several *in vitro* and *in vivo* models.

Material and methods

Human subjects

Human OA cartilage samples were obtained from 105 individuals (60.67 ± 5.901 years) who underwent total knee arthroplasty. The healthy cartilage specimens were sourced from 53 individuals (58.81 ± 5.571 years) undergoing amputation surgery due to necrosis or trauma of the lower extremity. Preoperatively, all the individuals underwent knee X-ray examination. The cartilage tissues were immediately snap-frozen in liquid nitrogen. The specimens were further processed for histological examination and were categorized according to the modified Mankin scoring system.[32] This study protocol was approved by the ethics committee of Zhongda hospital and full written consents were obtained before the operative procedure.

Inducible cartilage-specific conditional *Eldr* knockout and transgenic mice construction

$Eldr^{flox}$ mice were generated by Biocytogen with the CRISPR-Cas9-based EGE (extreme genome editing) system. After scanning the *Eldr* gene structure, transcripts, regulatory region, and conservation, the exons 4–6 of *Eldr* could be conditionally knocked out. We designed single-guide RNAs (sgRNAs) to target the introns 3–4 and the introns 6–7 by using the CRISPR design tool (http://www.sanger.ac.uk/htgt/wge/). Candidate sgRNAs were screened for on-target activity with the UCA Kit (Beijing Biocytogen), and two sgRNA with high specificity and on-target activity were chosen for the next step. The targeting vector was composed of a 1.5 kb 3′ homologous arm, *Eldr* exons 4–6 flanked by *loxP*, and a 1.5 kb 5′ homologous arm. The obtained $Eldr^{flox}$ founder mice were validated by PCR amplification and DNA sequencing. Heterozygous $Eldr^{flox/+}$ mice were obtained by crossing the founder mice and the wild-type (WT) C57BL/6 mice. Genotypes of F1 heterozygous $Eldr^{flox/+}$ mice were confirmed by PCR amplification, DNA sequencing, and Southern blot analysis. Col2a1-CreER^{T2} mice were purchased from Jackson Laboratories (Bar Harbor, ME, USA). To generate Col2a1-CreER^{T2};$Eldr^{flox/flox}$ mice, $Eldr^{flox/flox}$ mice were mated with Col2a1-CreER^{T2} mice to produce Col2a1-CreER^{T2};$Eldr^{flox/+}$ mice, which were then mated with $Eldr^{flox/flox}$ mice. The construction strategy of *Eldr ROSA26* knockin ($Eldr^{ROSA26}$) mice is similar with $Eldr^{\mathrm{flox}}$ mice and can be found in the supplemental information. All mice were housed under pathogen-free conditions with five or fewer mice per cage. Mice had free access to food and water. The mice used for all experiments were randomly assigned to control or treatment groups and to those used in OA evaluation. The experimental protocol was approved by and performed in accordance with protocols from the Institutional Animal Care and Use Committee of Southeast University.

lncRNA-mRNA microarray analysis and bioinformatics analysis

Arraystar Human lncRNA Microarray V4.0, which is designed for the global profiling of human lncRNAs and protein-coding transcripts, was used. About 40,173 lncRNAs and 20,730 coding transcripts can be detected. Differentially expressed lncRNAs and mRNAs between the two samples were identified through fold change filtering. Hierarchical clustering and gene set enrichment analysis (GSEA; https://gsea.org//) were implemented by R Package. Pathways of differentially expressed genes were analyzed by the KEGG database (http://www.kegg.jp/kegg/) and KOBAS software.[33] The secondary structure of *ELDR* and *ELDR*-binding motifs in *IHH* promoter were predicted by RNAstructure[34] and LongTarget,[35] respectively. To evaluate the chromatin accessibility landscape of the *IHH* promoter, we analyzed ATAC-seq data for human cartilage/chondrocyte from Cistrome Data Browser (GSM2895180, GSM2895184, GSM2895186, GSM2895188, GSM2895190, GSM2895179, GSM2895183, GSM2895185, GSM2895187, and GSM2895189). With respect to histone modifications of *IHH* promoter, ChIP-seq data for H3K4me3, H4K3me1, and H3K9ac from Cistrome Data Browser was analyzed (GSM670034, GSM670004, GSM669990, GSM670024, GSM670000, GSM669927, GSM670030, and GSM669917).

Solexa sequencing

Total RNA was extracted from cartilage samples (three WT mice versus three *ELDR* cKO (conditional knockout) mice; three WT mice versus 3 *ELDR* cKI (conditional knockin) mice. Using a NanoDrop ND-100 instrument, RNA was quantified. We used 1–2 μg total RNA to prepare the sequencing library. We employed oligo (dT) magnetic beads (rRNA removed) to enrich total RNA. The RNA sequencing (RNA-seq) library was prepared with a KAPA Stranded RNA-Seq LibraryPrep Kit (Illumina). Finally, the completed libraries were examined with Agilent 2100 Bioanalyzer and quantified by absolute quantification qPCR method. Subsequently, it was sequenced for 150 cycles for both ends on Illumina HiSeq instrument.

SA-β-galactosidase staining (SA-β-gal)

Chondrocytes were washed twice with PBS and fixed with 2% paraformaldehyde and 0.2% glutaraldehyde for 5 min. Fixed cells were washed and incubated with SA-β-gal staining solution (Cell Biolabs) at 37°C for 15 h. Subsequently, cells were washed with PBS and imaged with a light microscope. Total cells and SA-β-gal-positive cells were counted.

Telomere length measurement and telomere FISH

Genomic DNA was extracted directly from chondrocytes with a Mini Genomic DNA Kit (QIAamp DNA Mini Kits) according to manufacturer's protocols (Qiagen). Telomere length was determined with an RT-qPCR method. Telomere fluorescence *in situ* hybridization (FISH) was performed with a PNA (peptide nucleic acid) probe (Panagene).

RNAScope

We performed RNAScope assay to detect the single-molecule RNA by using the RNAScope Assay Kit (Advanced Cell Diagnostics, CA, USA). For targeting *ELDR*, 20 paired double-Z oligonucleotide probes were designed. The cultured human chondrocytes were fixed by 10% neutral formalin at room temperature for 30 min, incubated in a hydrogen peroxide solution for 15 min, and digested in protease III solution for 20 min. Subsequently, these cells were hybridized with target probes at 40°C for 2 h. Finally, the cells were conjugated with TSA Plus Cy3 fluorescence. The cells were counterstained with DAPI. Images were acquired with a confocal microscopy.

RNA *in situ* hybridization-proximity ligation assay (rISH-PLA)

The *in situ* proximity ligation assay (PLA) was performed on fixed primary proliferating chondrocytes with the DuoLink PLA fluorescence technology (Sigma-Aldrich #DUO92101) according to the manufacturer's protocol. Interaction between *ELDR* and hnRNPL or KAT6A was confirmed with the rISH-PLA assay. The oligonucleotides against *ELDR* were designed with the Stellaris design tool (https://www.biosearchtech.com/support/education/stellaris-rna-fish) (Cy3 labeled 5′-CAGCAAAAAAATGAGTGCCC TA-3′).

Cell culture and transfection

We employed human cartilage (OA affected and healthy controls) and cartilage from *Eldr* cKO, *Eldr*$^{flox/flox}$, *Eldr*^{ROSA26}, and *Eldr* cKI mice to isolate primary chondrocytes. In high glucose Dulbecco's modified Eagle's medium (DMEM) with 10% fetal calf serum (FCS), 100 IU/mL penicillin, and 100 μg/mL streptomycin, human chondrocytes, SW1353, and C28/I2 cells were maintained in a monolayer at 37°C in a 5% CO_2 environment. Then, these cells were transfected with antisense LNA GapmeR-*ELDR* or antisense LNA GapmeR control labeled or unlabeled with Cy3 at 10 mM via Lipofectamine RNAiMAX Transfection Reagent (Invitrogen, Life Technologies, Carlsbad, CA, USA). The pCDNA3.1 (Invitrogen) vector was sub-cloned with the synthesized *ELDR* sequence. Transfection of the pCDNA3.1-*ELDR*, *IHH*, *hnRNPL*, or *KAT6A* led to increased abundance of *ELDR*, IHH, hnRNPL, or KAT6A, with an empty pCDNA3.1 vector serving as the control (Invitrogen). siRNA targeting *hnRNPL* and *KAT6A* as well as a negative control siRNA were transfected into chondrocytes at a dose of 50 nM (Invitrogen, Life Technologies, Carlsbad, CA, USA).

RNA isolation, cDNA synthesis, and RT-qPCR

We employed TRIzol to isolate total RNA from cartilage samples and cultured cells (Ambion, Life Technologies). RNA quantity and quality were determined with a nanodrop (Thermo Fisher Scientific, Waltham, MA, USA) and Bioanalyzer (Agilent Inc., Santa Clara, CA, USA). After that, RNA was reverse-transcribed with the PrimeScript RT Reagent Kit (Takara Bio). Using an ABI QuantStudio 5 (Applied Biosystem, Foster City, CA, USA), we performed RT-qPCR. Relative gene expression (*ELDR* and other genes, normalized to endogenous control gene *β-actin* or *GAPDH*) was calculated with the comparative Ct method formula $2^{-\Delta\Delta Ct}$. The primer sequences used in this study are listed in Table S2.

Flow cytometry and 5-Ethynyl-2′-deoxyuridine (EdU) assay

We used an Annexin V-fluorescein isothiocyanate (FITC)/propidium iodide (PI) Kit (BD Biosciences, Franklin Lakes, NJ, USA) to analyze chondrocyte apoptosis. After 48 h of transfection, chondrocytes were harvested and incubated with Annexin V-FITC and PI in darkness for 20 min. After centrifugation, the cells were re-suspended by PBS and analyzed via flow cytometry.

For EdU assay, primary human chondrocytes were cultured and seeded onto 24-well plates. Then, 50 μM of EdU (Sigma-Aldrich) was added to each well for 2 h. Next, cells were fixed with 4% formaldehyde for 15 min, followed by permeabilization with 0.5% Triton X-100 for 20 min at room temperature. Subsequently, the cells were stained with Hoechst 33258. The EdU incorporation rate was expressed as the ratio of EdU-positive cells to total Hoechst 33258-positive cells.

3′- and 5′-rapid amplification of cDNA ends (RACE)

We conducted the 5′-RACE and 3′-RACE analyses to determine the transcriptional initiation and termination sites of *ELDR* by using a SMARTer RACE cDNA Amplification Kit (Clontech, Palo Alto, CA, USA). In brief, we isolated RNA from human chondrocytes and 3′- and 5′-RACE-ready cDNA were synthesized by using SMARTScribe Reverse Transcriptase. The following amplification procedures were used: five cycles at 94°C for 30 s at 72°C, five cycles at 94°C for 30 s at 70°C, and 25 cycles at 94°C for 30 s at 68°C. The resulting band underwent gel purification and pRACE vector linearization for cloning. After that, the acquired band was sequenced. The primer sequences used in this study are shown in Table S2.

Nuclear-cytoplasmic RNA fraction and FISH

Following the instructions provided by the manufacturer, we used the PARISTM Kit (Invitrogen) to isolate the cytoplasmic and nuclear RNA. Trypsin was employed to break down chondrocytes, and then chondrocytes were centrifuged at 1,200 rpm for 5 min. Centrifuging materials for 3 min at 500 g separated the cytoplasmic and nuclear cell fractions. Nuclear and cytoplasmic RNA were both eluted. Following that, cytoplasmic and nuclear RNA were purified and analyzed according to the RT-qPCR.

For FISH, digoxin (Dig)-conjugated LNA (lock nucleic acid) oligonucleotide probes were custom made and synthesized by Exiqon (QIAGEN). Anti-Dig fluorescein-conjugated antibody (13399600, Roche, dilution 1:200) was treated with chondrocytes overnight at 4°C. Chondrocytes were seeded and then treated with 0.5% Triton in PBS, 4% paraformaldehyde, and prehybridized. Overnight, the cells were hybridized with 10 M *ELDR*, *U6*, and 18S rRNA probes. The probes used in this study are listed in Table S3.

Serial deletion analysis and site-directed mutagenesis

We cloned full-length *ELDR* or mutant *ELDR* containing different deletions into the pcDNA3.1 vector for the RNA pull-down tests to enable *in vitro* transcription of biotin-labeled and unlabeled *ELDR*. The sequence has been provided in Table S4. We employed the QuikChange Site-directed Mutagenesis Kit (Stratagene, La Jolla, CA, USA) to create the mutant *ELDR* RNAs according to the instructions provided by the manufacturer. The serial deletion fragments of *ELDR* were amplified via either serial 3′ nested PCR primers with common 5′ primers or serial 5′ nested PCR primers with common 3′ primers.

RNA pull-down and RNA immunoprecipitation (RIP)

Using a Transcript Aid T7 High Yield Transcription Kit (Thermo Fisher Scientific), we obtained full-length *ELDR* and antisense sequences. Then, the sequences were treated with RNase-free DNase I and purified with the GeneJET RNA purification kit (Thermo Fisher Scientific). Nuclear extracts were prepared with the NE-PER Nuclear Protein Extraction Kit (Thermo Fisher Scientific). Meanwhile, recombinant *hnRNPL* or *KAT6A* was also used. RNA pull-down assays were performed with the Magnetic RNA-Protein Pull-down Kit (Thermo Fisher Scientific). Finally, the retrieved protein was separated on SDS-PAGE gels visualized with a silver staining or by immunoblot. The RIP assay was performed according to the manufacturer's protocol (the EZ-Magna

RIP Kit, Millipore, MA, USA). Normal mouse IgG was used as the negative control. For RT-qPCR analysis, *U1* RNA was used as a non-specific control.

Northern blot and RNA-electrophoretic mobility shift assay (EMSA)

Total RNA was extracted from chondrocytes with standard TRIzol methods and then subjected to electrophoresis with formaldehyde denaturing agarose gel. Samples were transferred to positively charged normal control (NC) film (Beyotime Biotechnology) with 20× saline sodium citrate (SSC) buffer (3.0M NaCl and 0.3M sodium citrate [pH 7.0]), followed by UV crosslinking. Membranes were incubated with hybrid buffer at 65°C for 20 h supplemented with digoxin-labelled RNA probes generated by *in vitro* transcription. Digoxin signals were detected with HRP-conjugated anti-digoxin antibody (Thermo Fisher Scientific).

The biotin-labeled *IHH* promoter fragment (−476 to −453 bp) was incubated with increasing amounts (0.4, 0.6, and 0.8 μL) of *in vitro* transcribed *ELDR* (1,138–1,152 nt) in 20 mM KCl, 40 mM Tris-acetate (pH 7.5), 10 mM Mg $(CH3COO)_2$, and 10% glycerol. Triplex formation was detected by EMSA on 12% polyacrylamide gels. The biotin-labeled *IHH* fragment and its complexes were detected with a LightShift chemiluminescent RNA EMSA Kit (Thermo Scientific, USA).

ChIP-qPCR and chromatin isolation by RNA purification (ChIRP)-qPCR analysis

According to manufacturer's instructions, the ChIP experiments were performed with EZ-Magna ChIP A/G kit (Millipore, Billerica, MA, USA). A total of 1×10^6 chondrocytes were fixed in 1% formaldehyde at room temperature for 10 min, and the nuclei were isolated with nuclear lysis buffer supplemented with a protease inhibitor. The chromatin DNA was cut into lengths ranging from 100 to 200 bp. The sheared chromatin was immunoprecipitated at 4°C overnight with an anti-hnRNPL antibody (Abcam), anti-H3K4me3 antibody (Cell Signaling Technology), anti-KAT6A antibody (Cell Signaling Technology, ChIP), anti-H3K9ac antibody (Abcam), anti-H3K4me1 antibody (Abcam), or anti-NRF1 antibody (Cell Signaling Technology). The primers of ChIP-qPCR are provided in Table S2.

The Magna ChIRP RNA Interactome Kit was obtained from Millipore (Millipore, MA, USA) and used according to the manufacturer's instructions. The probes used in the ChIRP-qPCR assay are listed in Table S3.

DNA pull-down

The region 600 bp upstream of the transcriptional start site of *IHH* was amplified by PCR with biotinylated primers. This probe was then mixed with the lysates from the chondrocytes and incubated at room temperature. Probe-protein complexes were precipitated with streptavidin-coupled DynaBeads (Thermo Fisher Scientific), and proteins were eluted with increasing NaCl concentrations (700 mM). Enriched proteins were subjected to SDS-PAGE, followed by immunoblot and mass spectrometry (Q Exactive mass spectrometer, Thermo Fisher Scientific).

Dual luciferase activity assay

We employed luciferase experiments to examine the relationship between the *IHH* promoter and either the *ELDR* or the *NRF1*. In order to transfect chondrocytes overexpressing *ELDR* or *NRF1*, we cloned the specified *IHH* promoter segments (between −2,000 bp and +200 bp) into the pGL3 plasmid (Promega, Madison, WI, USA). A negative control, the pGL3 vector, was utilized. A reporter plasmid containing Renilla luciferase was used as the standard reference. After 24 h transfection, the luciferase activities were detected following the instruction of the Dual-Luciferase Reporter Assay System (Promega, WI, USA). Renilla luciferase intensity was normalized against firefly luciferase intensity. All transfections were carried out in triplicate.

Molecular docking and molecular dynamics simulations

AMBER16 software[36] ran molecular dynamics simulations on the basis of the optimal docking conformation of the hnRNPL or KAT6A-*ELDR* complex. Before running the simulation, default protonation states at neutral scores were set to ionize the amino acids and add hydrogen atoms to the complex to initialize it via the leap module. To create complex topology files, we used AmberTools with the AMBER ff99sb force field and the TIP3P water model. The system was neutralized by the addition of Na+, and the last salt concentration reached 0.15 M. Under periodic boundary conditions, the simulation for molecular dynamics was run via the particle mesh Ewald (PME) method[37] with a 0.1 nm minimum distance to the box's edge. Bond lengths were all restricted via the Verlet leapfrog algorithm,[38] and the integration time step was set to 2 fs. We then employed a harmonic potential was then employed to restrain the hnRNPL or KAT6A-*ELDR* complex while the force constant for the form k $(\Delta x)^2$ was set to k = 100 kcal/mol $^{-1}$Å^{-2}. For the protein-*ELDR* complexes, a 10 ns MD simulation with a 2,000 ps time step was completed under the conditions of 298 K and 1 atm (atmosphere). For the final average structure of the hnRNPL- or KAT6A-*ELDR* complex, 5,000 snapshots total, extracted from the trajectory of the last 10 ns MD simulation, were used.

Immunoblotting

Protein lysates were prepared from cultured chondrocytes with RIPA buffer supplemented with protease and phosphatase inhibitors. We used the BCA Protein Assay Kit (Thermo Fisher Scientific) to determine the protein concentrations. Proteins were separated with 6%–12% SDS-PAGE gels and then transferred to polyvinylidene fluoride membrane. The membranes were subsequently probed with primary antibodies. After washing with TBS-T, the membranes were incubated with secondary antibodies. Immunocomplexes were visualized through chemiluminescence with an ECL (efficient chemiluminescence) kit (Amersham Biosciences). The uncropped blots are provided in Figure S8.

Cell immunofluorescence

Chondrocytes were cultured and treated on coverslips in 24-well plates. They were sequentially incubated with 4% formaldehyde, 0.5% Triton X-100, and 5% BSA in PBS, primary antibodies. The fluorescence was visualized under CarlZeiss LSM710 confocal microscope (CarlZeiss, Oberkochen, Germany). The percentage of positive cells was calculated by Image-Pro Plus 6.0.

X-ray and histological evaluation

Radiographs of mouse knee joints were obtained with the Faxitron MX20 X-ray system. The mouse joints were scanned and analyzed with the Skyscan 1176 micro-CT scanner (Skyscan, Aartselaar, Belgium). The tissues were embedded in paraffin, sectioned, and stained with hematoxylin-eosin (H&E), masson staining, safranin-O/fast green, and immunohistochemical assay. Decalcified cartilage was stained with safranin-O and scored with the OARSI grading system (grade 0–6).[39,40] Synovitis (grade 0–3) was determined by safranin-O and hematoxylin staining.[41,42]

Statistical analysis

Data are presented as the mean ± SEM or median (25th–75th percentiles), as indicated in figure legends. Before statistical analysis, normal distribution was determined via Shapiro-Wilk and Kolmogorov-Smirnov tests. We used unpaired t test or Mann-Whitney U test to compare two independent groups. In multiple comparisons, one- or two-way ANOVA followed by Tukey's post hoc test was used. Spearman's correlation analysis was performed. All statistical tests used were two sided. A p value less than 0.05 was considered statistically significant. All statistical analyses were performed with GraphPad Prism 8 (GraphPad Software Inc., La Jolla, CA, USA) and R software (version 4.2.1).

Results

ELDR is a cartilage senescence-associated lncRNA

To investigate lncRNA transcriptome changes during OA, we employed the Arraystar human lncRNA + mRNA Array V4.0 (8 × 60K format) to profile the lncRNA expression in cartilage tissues from three OA-affected individuals and three healthy control individuals. (Figures 1A and S1A). In general, noncoding RNA expression profile study can be divided into three phases, i.e., screening, one-stage validation, and two-stage validation.[43–45] This is a very reliable method in selecting noncoding RNA, probably because of the unique characteristics of noncoding RNAs.[46,47] We used a set of stringent criteria to filter lncRNAs, which refer to fold change > 10 (10 times higher than that in control group) or < 0.1 (10 times lower than that in control group) with a $p < 0.05$, >200 nucleotides (nt) in length, no overlap with protein-coding regions or pseudogenes,[48] and low predicted coding probability.[49] Finally, a total of 38 dysregulated lncRNAs (23 upregulated and 15 downregulated) were selected for further analysis (Figures 1B and 1C). We then tested these 38 lncRNAs by using an independent cohort of 21 control individuals and 42 OA-affected individuals. *SHANK2-AS2*, *ELDR*, *LINC01521*, *LINC01159*, and *RP11-802E16.3* were observed to be significantly dysregulated (Table S1). These five lncRNAs were further evaluated with an additional independent cohort comprising of 32 control individuals and 63 OA-affected individuals. Of the five lncRNAs, *LINC01521* and *ELDR* were found to be significantly upregulated in OA-affected individuals compared with control individuals (Table S1). Finally, we focused on the most highly upregulated, *ELDR*, for further investigation. *ELDR* expression was determined in cartilage tissues from 105 human OA-affected individuals and 53 healthy control individuals (Figure 1D, i). Meanwhile, *ELDR* expression was also detected in chondrocytes of human OA-affected individuals and healthy control individuals (Figure 1D, ii). These results all indicated high expression level of *ELDR* in human OA.

ELDR is located at human chromosome 7p11.2, harboring four exons, and is highly conserved in different species (Figures S1B and S1C). Notably, *ELDR* was specifically elevated in human cartilage (Figure S1D). However, the shorter form of *ELDR* was not detected in human cartilage (Figure S1E). We performed 5′ and 3′ RACE and found a transcript of *ELDR* that contains 2,724 nucleotides with a poly(A) tail, which is transcribed from exons 1, 3, and 4 (Figures S1F and S1G) and which was not annotated in the UCSC Genome Browser, Ensembl, or LNCipedia. The full length (2,724 nt) was further validated by northern blot (Figure S1H). Moreover, the noncoding nature of *ELDR* was confirmed by coding potential calculator (CPC)[50] and coding-potential assessment tool (CPAT) analysis[51] (Figure S1I). To determine the abundance of *ELDR* in chondrocytes, we examined the copy number of *ELDR*. The result demonstrated that the copy numbers of *ELDR* were higher in chondrocytes from OA-affected individuals (Figure S1J). Furthermore, RNAScope assay (Figure 1E) and FISH (Figure S1K) showed that *ELDR* located primarily in the nucleus.

The profile of dysregulated mRNAs was also analyzed in OA (Figure S1L). All these genes were subjected to Gene Ontology (GO) analysis. Upregulated genes were related to replicative senescence (GO: 0090399), tumor necrosis factor-activated receptor activity (GO: 0005031), and interleukin-6 receptor complex (GO: 0005896) (Figure S1L), indicating the important role of cellular senescence in human OA. Importantly, levels of the senescence markers p16^{INK4a}, TNF-α, IL-1β, and IL-6 were markedly elevated in OA compared to controls (Figure 1F), further confirmed by RT-qPCR analysis in cartilage tissues and chondrocytes (Figures S1M and S1N). We quantified telomere length in chondrocytes isolated from human OA, and telomere maintenance was not observed in osteoarthritic chondrocytes (Figure 1G). Increased senescence-associated-galactosidase (SA-β-Gal) positivity was also found in OA (Figure 1H). Given the key role of lncRNAs in cellular senescence,[4] we explored a possible association between *ELDR* and chondrocyte senescence. The correlation analysis showed that *ELDR* expression level significantly correlated with the modified Mankin scale, p16^{INK4a}, TNF-α, IL-1β, and IL-6 levels (Figure S1O). These data imply that the novel transcript of *ELDR* may play an important role in osteoarthritic phenotype.

The critical role of *Eldr* in embryonic chondrocyte senescence

To investigate the involvement of *Eldr* in embryonic chondrocyte senescence, *Eldr* knockout and *Eldr ROSA26* knockin (KI) mice were constructed with the CRISPR-Cas9 based EGE system (Figures S2A–S2F). We then crossed Col2a1-CreER^{T2} mice with *Eldr*$^{flox/flox}$ and *Eldr*^{ROSA26} mice to generate chondrocyte-specific *Eldr* KO and KI mice. Pregnant mice with embryos at embryonic day 10.5 (E10.5) were injected with tamoxifen. Notably, the size of *Eldr* cKI mice skeleton was smaller than that of *Eldr*

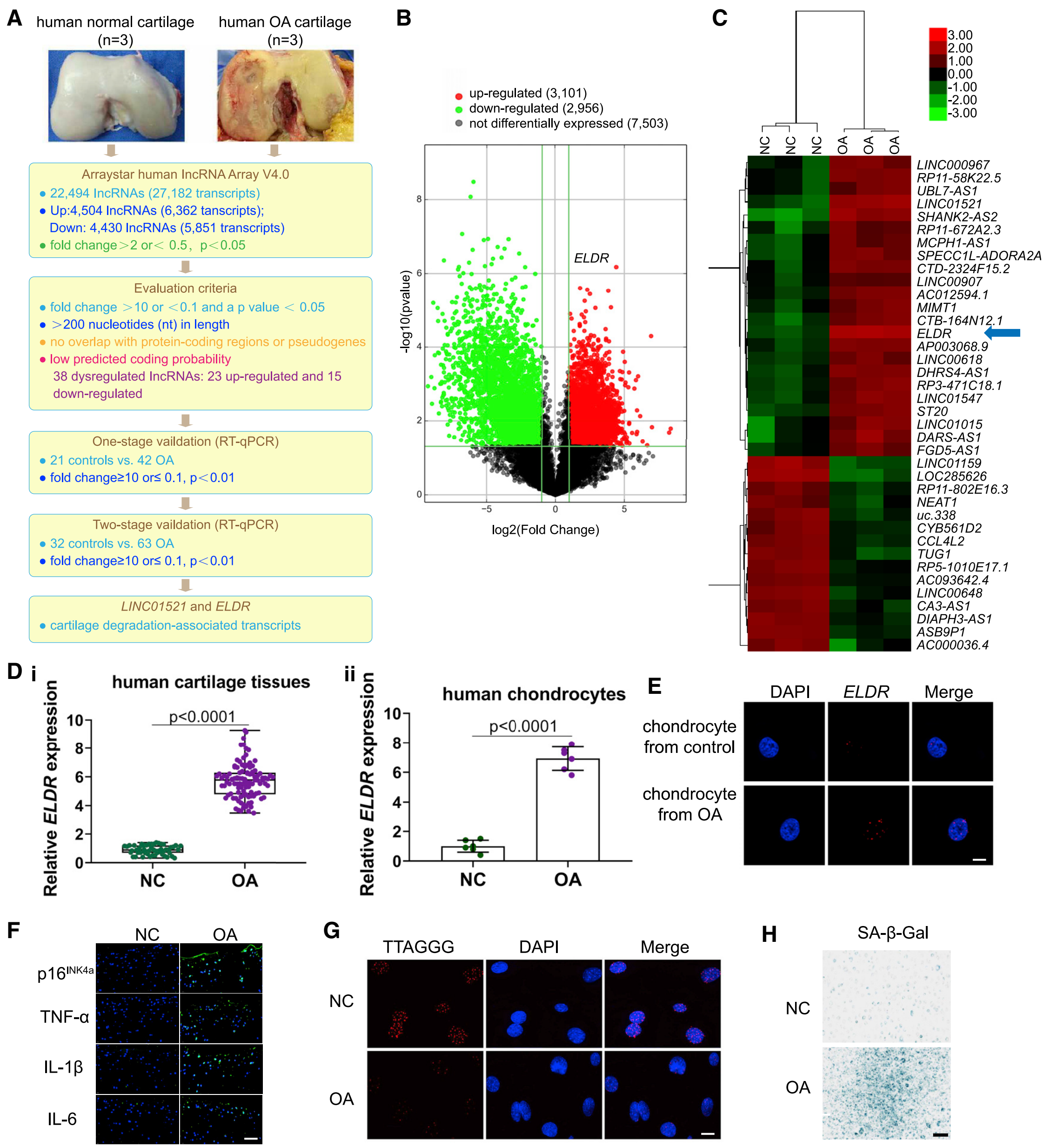

Figure 1. Systematic identification of senescence-associated lncRNAs in human OA
(A) Overview of lncRNA selection strategy for transcriptome analysis of cartilage from OA-affected individuals (n = 3) and controls (n = 3).
(B) Volcano plot showing differentially expressed lncRNAs.
(C) The heatmap depicting 38 differentially expressed lncRNAs.
(D) RT-qPCR analysis of *ELDR* expression in human OA (n = 105) and control (n = 53) cartilage tissues (i). In addition, the *ELDR* expression level was also determined in human chondrocytes from OA-affected and control individuals (ii). n = 6 biological replicates per group.
(E) RNAScope demonstrating subcellular localization and relative expression of *ELDR* (red) in chondrocytes from OA-affected individuals and control individuals.
(F) The representative images of immunostaining of $p16^{INK4a}$, TNF-α, IL-1β, and IL-6 in human cartilage tissues. n = 3 biological replicates per group.
(G) Representative fluorescence microscopy images of telomere FISH analysis in human primary chondrocytes. n = 6 biological replicates per group.
(H) Representative images of SA-β-Gal staining of human primary chondrocytes. n = 3 biological replicates per group. Scar bar: 10 μm (E and G), 20 μm (F), 100 μm (H). Graphs are presented as the mean ± SEM (D, ii) or median (25^{th}–75^{th} percentiles) (D, i). p values are from two-tailed Mann-Whitney U test (D, i) and two-tailed unpaired Student's t test (D, ii).

cKO embryos as a result of cartilage dysregulation in the joints and intervertebral discs (Figures 2A and 2B). Intriguingly, we found that protein accumulation of $p16^{INK4a}$, p21, p53, and SASPs (Il-6, Tnf-α, and Mmp3) was upregulated at E14.5 and E18.5 of *Eldr* cKI mice compared with *Eldr* cKO mice (Figures S2G and S2H). Further, high levels of $p16^{INK4a}$ and p21 in *Eldr* cKI mice were confirmed by immunofluorescence staining (Figures 2C and 2D). At

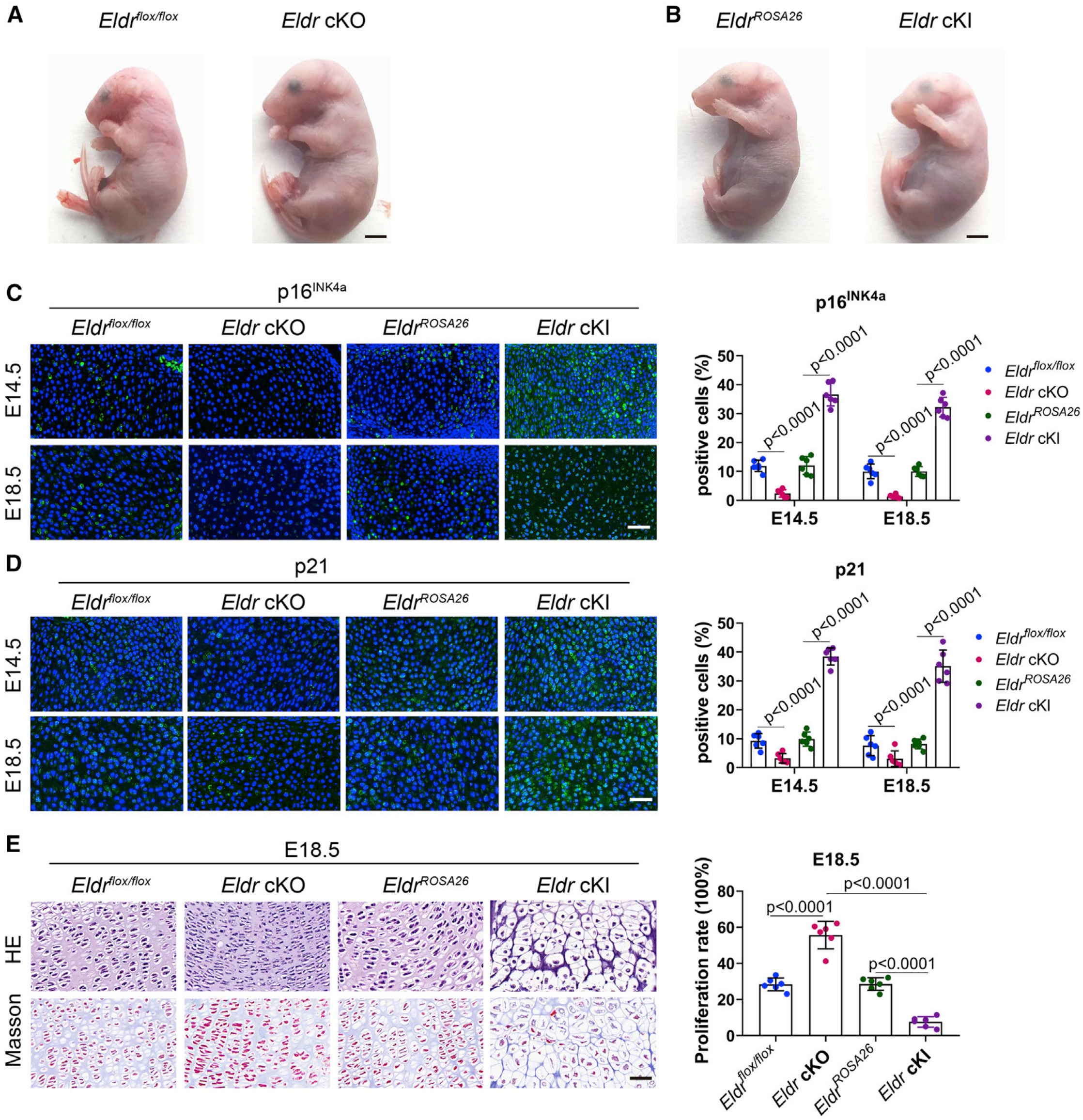

Figure 2. ***Eldr*** **regulates cartilage development and embryonic chondrocyte senescence**
(A) Gross appearance of *Eldr*$^{flox/flox}$ and *Eldr* cKO (E18.5). n = 6 embryos per group.
(B) Gross appearance of *Eldr ROSA26* KI and *Eldr* cKI (E18.5). n = 6 embryos per group.
(C) The immunofluorescence staining of p16^{INK4a} in cartilage tissues of tibias from *Eldr*$^{flox/flox}$, *Eldr* cKO, *Eldr*^{ROSA26}, and *Eldr* cKI mice embryo at E14.5 and E18.5. n = 6 mice per group.
(D) The immunofluorescence staining of p21 in cartilage tissues of tibias from the indicated mice embryo at E14.5 and E18.5. n = 6 mice per group.
(E) Representative images of H&E and Masson staining in cartilage tissues of tibias from the indicated mice embryo (E18.5). n = 6 mice per group. Scale bar: 1 mm (A and B), 50 μm (C–E). All graphs are presented as the mean ± SEM. p values are from one-way ANOVA test followed by Tukey's post hoc (p16^{INK4a} in E14.5 of C, D, and E) and Brown-Forsythe and Welch ANOVA test followed by Tamhane's T2 post hoc analysis (p16^{INK4a} in E18.5 of C).

E14.5 and E18.5, chondrocytes in proliferative zone of *Eldr* cKO mice had relatively high proliferation compared with *Eldr* cKI mice (Figures 2E and S2I). A further study should be performed to analyze whether those senescent chondrocytes that lost senescent hallmarks during embryogenesis can re-enter cell cycle or survive in the cartilage after birth. Taken together, these findings reveal that *Eldr* plays a key role in maintaining chondrocyte metabolism and determining the fate of senescent chondrocytes during embryogenesis.

Eldr regulates aging and injury-induced chondrocyte senescence during OA

Chondrocyte senescence is thought to be an important biological process that contributes to extracellular matrix remodeling that accelerates the course of age-related and post-traumatic OA.[2,3,15,52–54] On the basis of a CRISPR-Cas9-based EGE system, we established *Eldr* KO and *Eldr ROSA26* KI mice in order to study the function of *Eldr* in chondrocyte senescence *in vivo*. Then, we crossed Col2a1-CreER^{T2} mice with *Eldr*$^{flox/flox}$ and *Eldr*^{ROSA26} mice

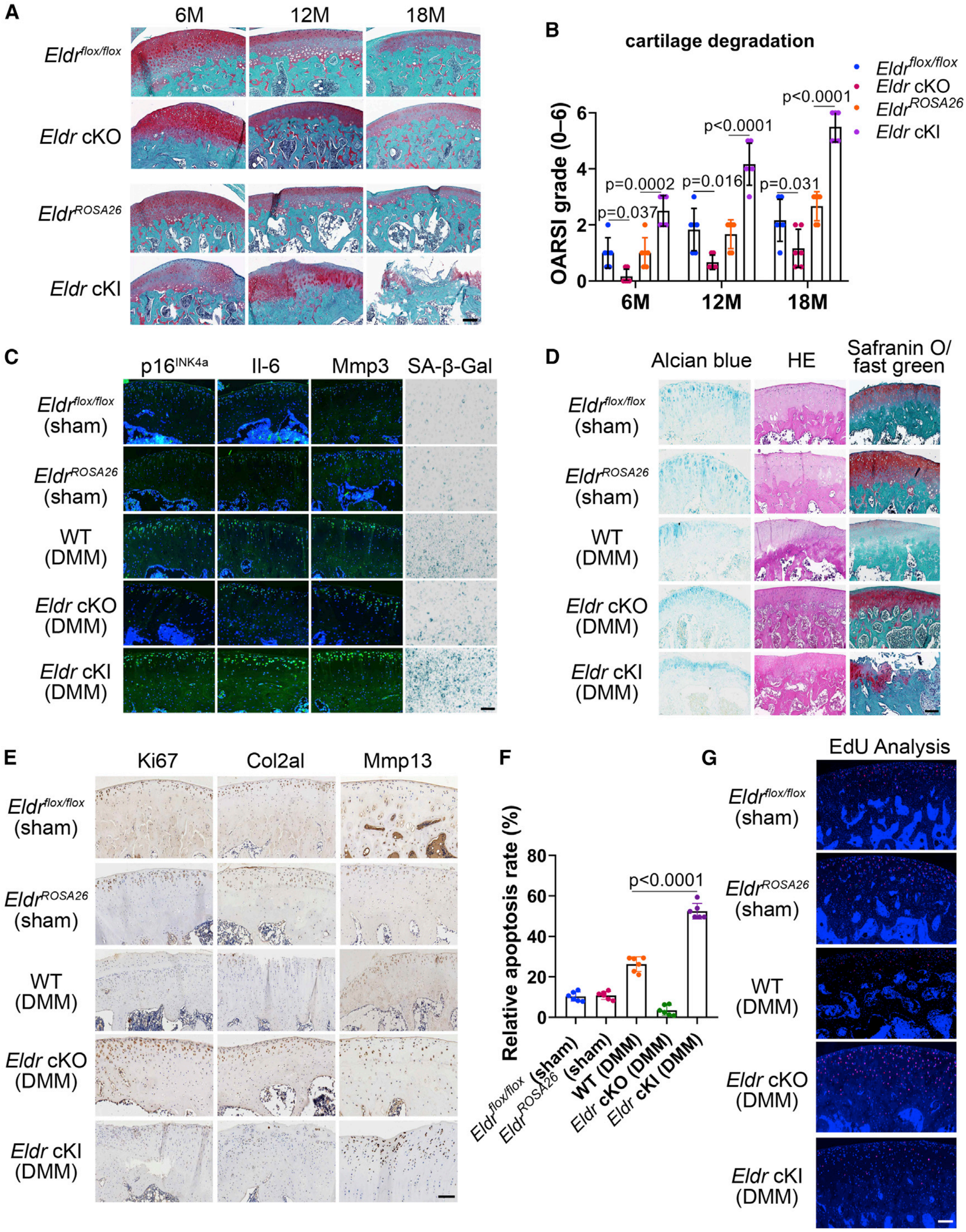

Figure 3. *Eldr* contributes to aging and injury-induced chondrocyte senescence

(A) Representative images of safranin-O staining of cartilage tissues from 6-month-old mice, 12-month-old mice, and 18-month-old mice (*Eldr*$^{flox/flox}$, *Eldr* cKO, *Eldr*^{ROSA26}, *Eldr* cKI). n = 6 mice per group.

(B) Histological evaluation (Osteoarthritis Research Society International, OARSI) was analyzed in aging mice (*Eldr*$^{flox/flox}$, *Eldr* cKO, *Eldr*^{ROSA26}, *Eldr* cKI). n = 6 mice per group.

(C) Representative images of immunostaining of p16^{INK4a}, Il-6, and Mmp3 in cartilage tissues and SA-β-Gal staining in chondrocytes from the indicated groups (*Eldr*$^{flox/flox}$ and *Eldr*^{ROSA26} mice undergoing sham surgery; WT, *Eldr* cKO, and *Eldr* cKI mice subjected to DMM surgery) at 8 weeks after surgery. n = 6 mice per group.

(D) Representative images of Alcian blue, H&E, and safranin-O/fast green staining in cartilage tissues from the indicated groups. n = 6 mice per group.

(E) Immunohistochemistry of ki67, Col2a1, and Mmp13 localization in cartilage tissues from mice (*Eldr*$^{flox/flox}$ and *Eldr*^{ROSA26} mice undergoing sham surgery; WT, *Eldr* cKO, and *Eldr* cKI mice subjected to DMM surgery). n = 6 mice per group.

(legend continued on next page)

to generate chondrocyte-specific *Eldr* KO and KI mice. We observed spontaneously developed OA in *Eldr* cKO and *Eldr* cKI mice with aging (Figure S3A). Tamoxifen (100 g/g body weight) was given intraperitoneally into $Eldr^{flox/flox}$, *Eldr* cKO, $Eldr^{ROSA26}$, and *Eldr* cKI (8-week-old) mice daily for 5 days. It should be noted that as compared to *Eldr* cKO mice, histological investigation of postnatal 6 months (P6M) *Eldr* cKI mice revealed some loss of proteoglycans, roughening of the articular cartilage, and a loss of cellularity in the articular chondrocytes (Figure 3A). By P12M, *Eldr* cKI animals had a higher loss of proteoglycans, a loss of cellularity, and degradation in specific areas of the articular cartilage (Figure 3A). By P18M, *Eldr* cKI mice showed more severe osteoarthritic phenotype, which was confirmed by the significant increase in the OARSI (Figure 3B) and synovitis score (Figure S3B). Subsequently, in WT, *Eldr* cKO, and *Eldr* cKI mice, we surgically destabilized the medial meniscus to develop post-traumatic OA. Senescence markers were considerably higher in *Eldr* cKI mice as compared to WT and *Eldr* cKO mice (Figures 3C and S3C). Intriguingly, *Eldr* cKO mice exhibited markedly reduced OARSI grading and significantly lower synovitis scores at 8 weeks after destabilizing the medial meniscus (DMM) surgery (Figures 3D and S3D). Immunohistochemistry staining showed protein localization of Ki67, Col2a1, and Mmp13 in indicated groups (Figures 3E and S3E). Furthermore, *Eldr* cKO animals showed considerably less chondrocyte apoptosis (Figures 3F, S3F, and S3G). Significant increase in the number of EdU+ chondrocytes was found in *Eldr* cKO mice cartilage, compared with other groups (Figures 3G and S3H). During OA development, *Eldr* was highly expressed (Figure S3I). These findings suggest that aging- and injury-induced SnCs share similar pathways because deletion of *Eldr* suppresses chondrocyte senescence as well as SASP *in vivo*.

ELDR **forms an RNA-DNA triplex with the** ***IHH*** **promoter region**

A detailed understanding of how chondrocytes enter the senescent state might enable the development of therapies designed to prevent such a phenotypic switch during OA.[1–4] Therefore, we looked into transcriptional targets regulated by *Eldr* that could be responsible for chondrocyte senescence during the development of OA. Using *Eldr* cKO and cKI mice chondrocytes, we performed RNA-seq analysis. The enriched genes in *Eldr* cKO chondrocytes were involved in extracellular matrix component lubricating action (GO: 0030197), extracellular matrix that contains collagen (GO: 0062023), and control of cartilage formation (GO: 0061035) (Figure S4A). In *Eldr* cKI chondrocytes, the enriched genes were related to cellular senescence (GO: 0090398), DNA repair complex (GO: 1990391), and chemokine activity (GO: 0008009) (Figure S4B). The findings imply that *Eldr* plays a key role in maintaining the homeostasis of chondrocytes. Five genes were found to be considerably dysregulated among these genes regulated by *Eldr*, which have been previously reported to be linked to OA.[12,13,55–57] RT-qPCR was then employed to quantify these genes. The results showed that *Hpip*, *Itgbl1*, and *Ihh* were downregulated in *Eldr* cKO chondrocytes and upregulated in *Eldr* cKI chondrocytes (Figure S4C). The hedgehog signaling pathway was clearly dysregulated, as shown by KEGG pathway analysis (Figures 4A and 4B). More notably, *Eldr* cKI in chondrocytes dramatically upregulated protein accumulation of Ihh, Ptch1, Gli, $p16^{INK4a}$, Tnf-α, Il-1β, Il-6, Mmp13 as well as Adamts5 while downregulating protein levels of Hmgb1, Col II, and Aggrecan (Figure S4D). In *Eldr* cKO chondrocytes, the findings were the exact reverse (Figure S4D). To further confirm the effect of *Eldr* knockdown on hedgehog pathway, we performed a rescue experiment by transfecting *Eldr* cKO chondrocytes with pCDNA3.1-Ihh. The inhibition of the hedgehog pathway, senescent markers, and SASP expressions by *Eldr* knockdown were partially rescued by restoration of *Ihh* expression (Figure S4E). These results provide direct evidence that Ihh plays a vital role in *Eldr*-induced chondrocyte senescence.

It is noteworthy that *IHH* is not located on the same chromosome as *ELDR* (Figure S4F). Further, we found that *Eldr* depletion had no effect on the expression of nearby genes (Figure S4F). Given the relationship between *Eldr* and *Ihh* (Figures S4D and S4E), *Eldr* could regulate *Ihh* in *trans*. We thus conducted FISH and subcellular fractionation tests to further understand the processes underpinning expression of *ELDR*-induced *IHH*, and the results showed that *ELDR* was mostly localized to the nucleus (Figures S4G and S4H). To explore whether *ELDR* transcriptionally upregulated *IHH*, we generated a series of *IHH-luc* promoter constructs, located from −2,000 bp upstream to +200 bp downstream of the transcriptional start site. As demonstrated in Figure 4C, the promoter luciferase assay showed that the −550 to +200 bp region of the *IHH* promoter led to an obvious increase of transcriptional activity. Furthermore, ChIRP assay showed that *ELDR* interacted physically with the area of the *IHH* promoter between −476 and −453 bp (Figures 4D, 4E, and S4I). Using LongTarget, we predicted five probable pairs of triplex-forming oligonucleotides (TFOs) and their associated triplex target sites (TTSs) in the *ELDR* and *IHH* promoter, respectively. Both fluorescence resonance energy transfer (FRET) and circular dichroism (CD) spectroscopy were performed on every binding motif. Compared with that of the control ssRNA/*IHH* TTS group (Figure S4J, i), FRET demonstrated an obvious increase in fluorescence intensity at

(F) Chondrocytes apoptosis was assayed in the indicated groups ($Eldr^{flox/flox}$ and $Eldr^{ROSA26}$ mice undergoing sham surgery; WT, *Eldr* cKO, and *Eldr* cKI mice subjected to DMM surgery). n = 6 mice per group.
(G) EdU analysis in cartilage sections from the indicated groups. n = 6 mice per group. Scale bar: 50 μm (A, C, D, E, and G). All graphs are presented as the mean ± SEM. p values are from one-way ANOVA test followed by Tukey's post hoc (B and F).

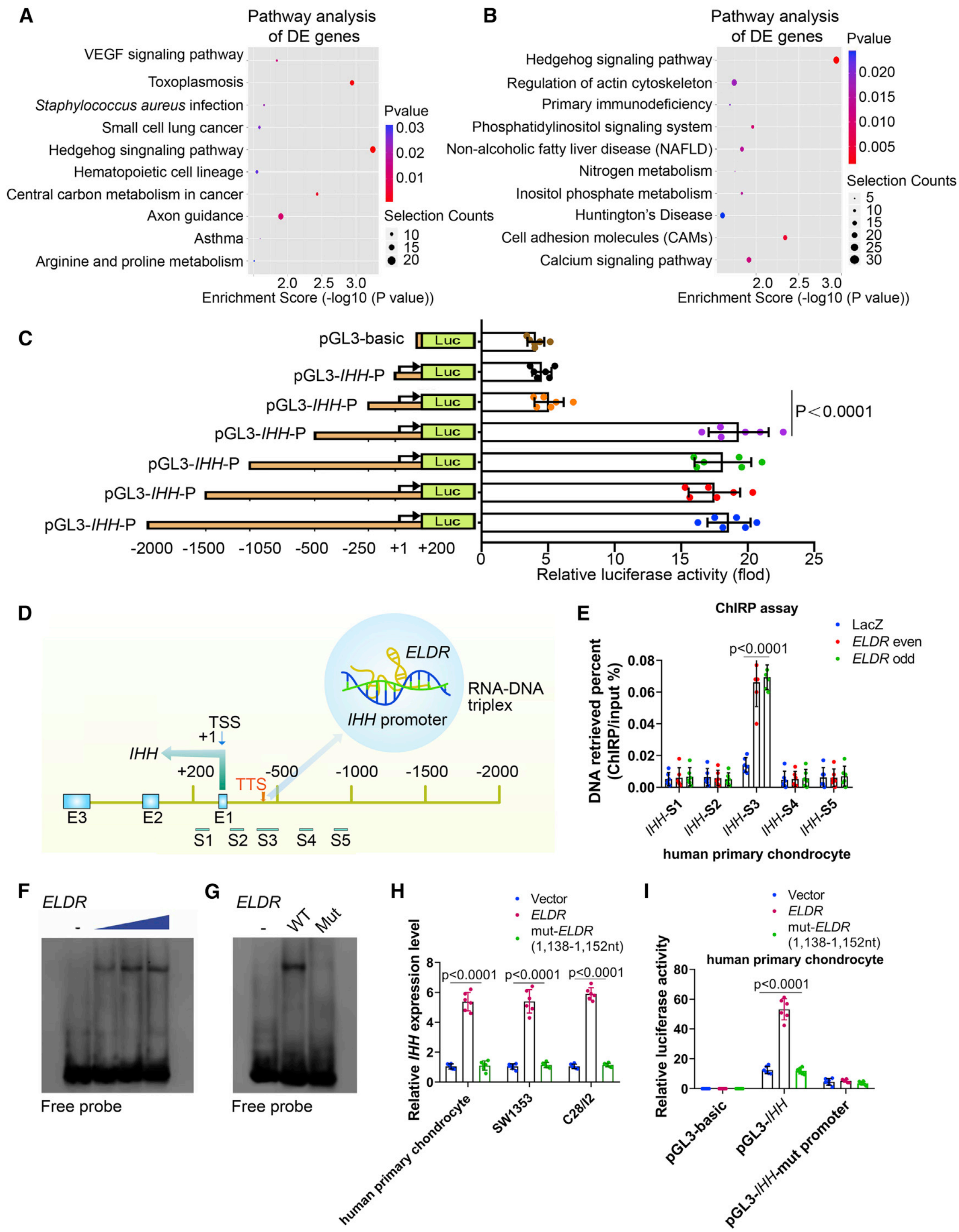

Figure 4. *ELDR* directly binds to the *IHH gene* promoter sequence
(A) KEGG analysis demonstrating hedgehog signaling pathway enriched in cartilage development.
(B) KEGG analysis showing hedgehog signaling pathway enriched in cartilage senescence.
(C) Transcriptional activity of the *IHH* promoter was evaluated using sequential deletions and the Renilla luciferase activity in human primary chondrocytes. n = 6 biological replicates per group.
(D) Schematic demonstration of the potential *ELDR* binding sites in the *IHH* promoter region. TSS, transcription start sites; TTS, triplex target sites.
(E) ChIRP-qPCR analysis of *ELDR*-associated chromatin in human primary chondrocytes. n = 6 biological replicates per group. "Even" and "odd" indicate the number of probes.
(F) Increasing amounts (0.4, 0.6, and 0.8 μL) of *ELDR* were incubated with double-stranded biotinylated *IHH* promoter, and formation of RNA-DNA triplexes was detected by EMSA.
(G) WT *ELDR* or mutant *ELDR* (1,138–1,152 nt) was incubated with double-stranded biotinylated *IHH* promoter, and the formation of RNA-DNA triplexes was confirmed by EMSA.

(legend continued on next page)

570–580 nm and a decrease at 520 nm in the *ELDR* (1,138–1,152 nt)/*IHH*-TTS1 (−476 to −453 bp) group (Figure S4J, iii). This result was similar to the FENDRR/PITX2-positive group (Figure S4J, ii). Compared with that of the control ssRNA/*IHH* TTS group (Figure S4K, i), CD displayed that the *ELDR* (1,138–1,152 nt)/*IHH*-TTS1 (−476 to −453 bp) group had a strong positive peak at 270–280 nm and a deep negative peak at 210 nm (Figure S4K, iii), which was similar to the FENDRR/PITX2-positive group (Figure S4K, ii). These results suggested that *ELDR* formed triplexes with promoter sequences of *IHH in vitro*. We performed an EMSA by using a biotinylated *IHH* TTS as the probe to further validate the triplex formation of *ELDR* on the *IHH* promoter. The result showed that *ELDR* could form complexes with the promoter (Figure 4F). Additionally, mutant *ELDR* (1,138–1,152 nt) was unable to bind to the *IHH* promoter (Figure 4G). As shown in Figure S4L, the DNA-RNA complexes were not disrupted by RNase H treatment, excluding the possibility that the band shift occurred as a result of DNA-RNA heteroduplexes. Mutated *ELDR* at 1,138–1,152 nt was unable to promote *IHH* expression (Figure 4H). Additionally, *ELDR* increased the *IHH* promoter's luciferase activity while the mutated *IHH* promoter showed no discernible change (Figures 4I and S4M), demonstrating the importance of the sequence between 1,138 and 1,152 nt in *ELDR* and −476 to −453 bp within the *IHH* promoter. These findings imply that *ELDR* regulates *IHH* transcription by creating a direct triplex formation with the promoter sequence.

We examined the 5′ and intron sequences of *ELDR*, an EGFR long noncoding downstream RNA, to identify the upstream factor regulating *ELDR* during chondrocyte senescence. We found three canonical EGFR binding sites (E-boxes) in this region (Figure S4N), raising the possibility that *ELDR* is an EGFR direct target. Transcriptional regulation of *ELDR* was downregulated or increased, respectively, when *EGFR* was knocked down or overexpressed (Figure S4O). It was shown by a luciferase activity experiment that EGFR may directly encourage *ELDR* transcription. In contrast to enhancers, a promoter's activity often depends on orientation (Figure S4P). Additionally, ChIP-qPCR showed that EGFR was found to robustly bind to the tandem E-boxes of 5′ and 3′ in the *ELDR* promoter (Figure S4Q). Together, these findings demonstrate that *ELDR* is an EGFR direct target.

ELDR recruits hnRNPL and KAT6A to the *IHH* promoter and promotes methylation of H3K4 and acetylation of H3K9

lncRNAs can bind to transcription factors, histone regulators, or other cellular factors to modulate downstream gene expression, serving as scaffolds for the histone modification complex.[58,59] Subsequently, we performed an RNA pull-down assay to identify *ELDR*-interacting proteins in chondrocytes. Two bands at about 64 and 225 kDa were specifically enriched in the *ELDR* pull-down proteins (Figure 5A). Using mass spectrometry, we identified hnRNPL and KAT6A as the most abundant *ELDR*-interacting proteins (Figure S5A). Immunolot further indicated that *ELDR* bound specifically to hnRNPL and KAT6A (Figures 5B and S5B). Of importance, RNA *in situ* hybridization-proximity ligation assay (rISH-PLA) showed the proximity of *ELDR* to endogenous hnRNPL or KAT6A in the nucleus of human chondrocyte (Figure 5C) and SW1353 (Figure S5C). Consistently, RIP assays also demonstrated that *ELDR* directly interacted with hnRNPL and KAT6A (Figures 5D and S5D). To identify the key region of *ELDR* that can interact with hnRNPL and KAT6A, we performed serial deletion analysis. The results demonstrated that exon 4 of the *ELDR* transcript (1,640–1,680 nt) was necessary and sufficient to bind hnRNPL and KAT6A (Figure 5E), which was further confirmed by sliver staining (Figure 5F), RNA pull-down, and immunoblotting (Figure S5E) and RNA EMSA (Figure 5G). On the basis of minimum free energy (MFE), *ELDR* secondary structure was predicted by RNAstructure software.[34] The RNA-binding protein (RBP) binding site for hnRNPL and KAT6A was located in the 1,600–1,700 nt region of exon 4 of *ELDR* within a stem-loop structure (Figure S5F). The direct interaction of exon 4 of the WT *ELDR* transcript with hnRNPL and KAT6A was determined by molecular dynamics trajectory (Figures 5H, S5G, and S5H). To further confirm the exact domain of hnRNPL or KAT6A bound to *ELDR*, we constructed vectors carrying HA-tagged full length or truncation mutants of hnRNPL (FL, 1–589), (T1, 20–212), (T2, 80–212), and (T3, 1–86) and KAT6A (FL, 1–2,004), (T1, 30–305), (T2, 60–305), and (T3, 1–39). We performed RNA pull-down assay by using *in vitro* synthesized biotinlabeled full-length *ELDR* to examine its interaction with different constructs of *hnRNPL* or *KAT6A* ectopically expressed in chondrocytes. For hnRNPL, *ELDR* mainly interacts with the 87–212 residues that contain an "RRM1" domain. For KAT6A, *ELDR* mainly interacts with the 40–305 residues that contain a region required for nuclear localization (52–166) (Figure 5I).

After site-directed mutagenesis of this region, RIP was performed. The result revealed that it was critical for the interaction between *ELDR*, hnRNPL, and KAT6A (Figures S5I and S5J). hnRNPL and KAT6A epigenetically regulate target gene expression by association with H3K4me3 and H3K9ac.[60] To further elucidate the molecular mechanism for how *ELDR* regulates *IHH* expression, we performed ChIP-qPCR. The results showed *ELDR* overexpression

(H) The effects of overexpression of WT or site-directed mutagenesis of *ELDR* (1,138–1,152 nt) on IHH level were investigated using RT-qPCR in human primary chondrocytes. n = 6 biological replicates per group.
(I) *IHH* WT or mutated type (−476 to −453 bp) with WT or site-directed mutagenesis of *ELDR* (1,138–1,152 nt) were subjected to luciferase reporter assays in human primary chondrocytes. n = 6 biological replicates per group. All graphs are presented as the mean ± SEM. p values are from one-way ANOVA test followed by Tukey's post hoc (C, E, H, and I).

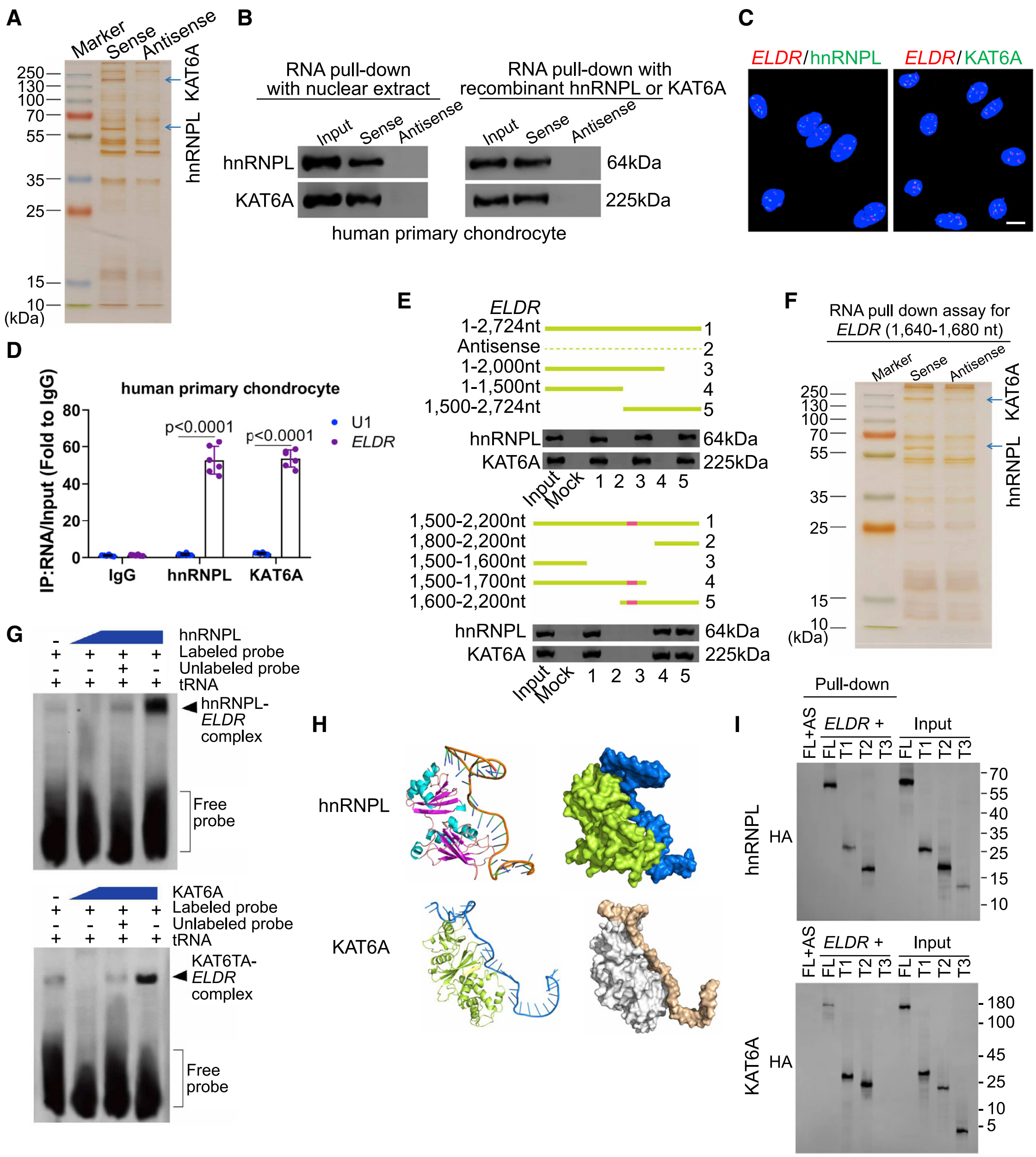

Figure 5. *ELDR*/hnRNPL/KAT6A promotes methylation of H3K4 and acetylation of H3K9 of the *IHH* promoter

(A) Representative image of silver-stained PAGE gels showing separated proteins that were pulled-down using biotin-labeled *ELDR* and arrows indicate hnRNPL and KAT6A.

(B) Immunoblot and pull-down were performed for further validation of hnRNPL and KAT6A.

(C) RNA *in situ* hybridization-proximity ligation assay (rISH-PLA) detects the close proximity of a specific RNA with proteins *in situ*. rISH-PLA confirms the proximity of *ELDR* to endogenous hnRNPL or KAT6A in the nucleus of cultured human primary chondrocyte.

(D) RIP analysis using the anti-hnRNPL or KAT6A antibody revealed that *ELDR* interacted with endogenous hnRNPL and KAT6A in human primary chondrocytes. *U1* was used as the negative control. n = 6 biological replicates per group.

(E) Serial deletions of *ELDR* were performed in the RNA pull-down assays to identify the core regions of *ELDR* for the physical interaction with hnRNPL and KAT6A.

(F) An RNA pull-down assay was performed using *ELDR* sense and antisense RNAs in human chondrocytes, followed by silver staining.

(G) hnRNPL or KAT6A and biotin-labelled key fragment of *ELDR* transcript (1,640–1,680 nt) were incubated for RNA EMSA assay.

(H) Interaction model between *ELDR* (1,640–1,680 nt) and hnRNPL or KAT6A.

(I) RNA pull-down showing the interaction between *ELDR* and HA-tagged full length or truncation mutants of hnRNPL (FL, 1–589), (T1, 20–212), (T2, 80–212), and (T3, 1–86) and KAT6A (FL, 1–2,004), (T1, 30–305), (T2, 60–305), and (T3, 1–39). AS (antisense) was used as a negative control. Bar: 10 μm (C). All graphs are presented as the mean ± SEM. p values are from two-tailed unpaired Student's t test (D).

dramatically enhanced hnRNPL and KAT6A occupancy at the *IHH* promoter and increased H3K4me3 and H3K9ac of the *IHH* promoter (Figures S5K and S5L). In comparison, mutated *ELDR* drastically attenuated this phenomenon (Figures S5I and S5J). Moreover, silencing hnRNPL or KAT6A inhibited transcriptional activation of *IHH* triggered

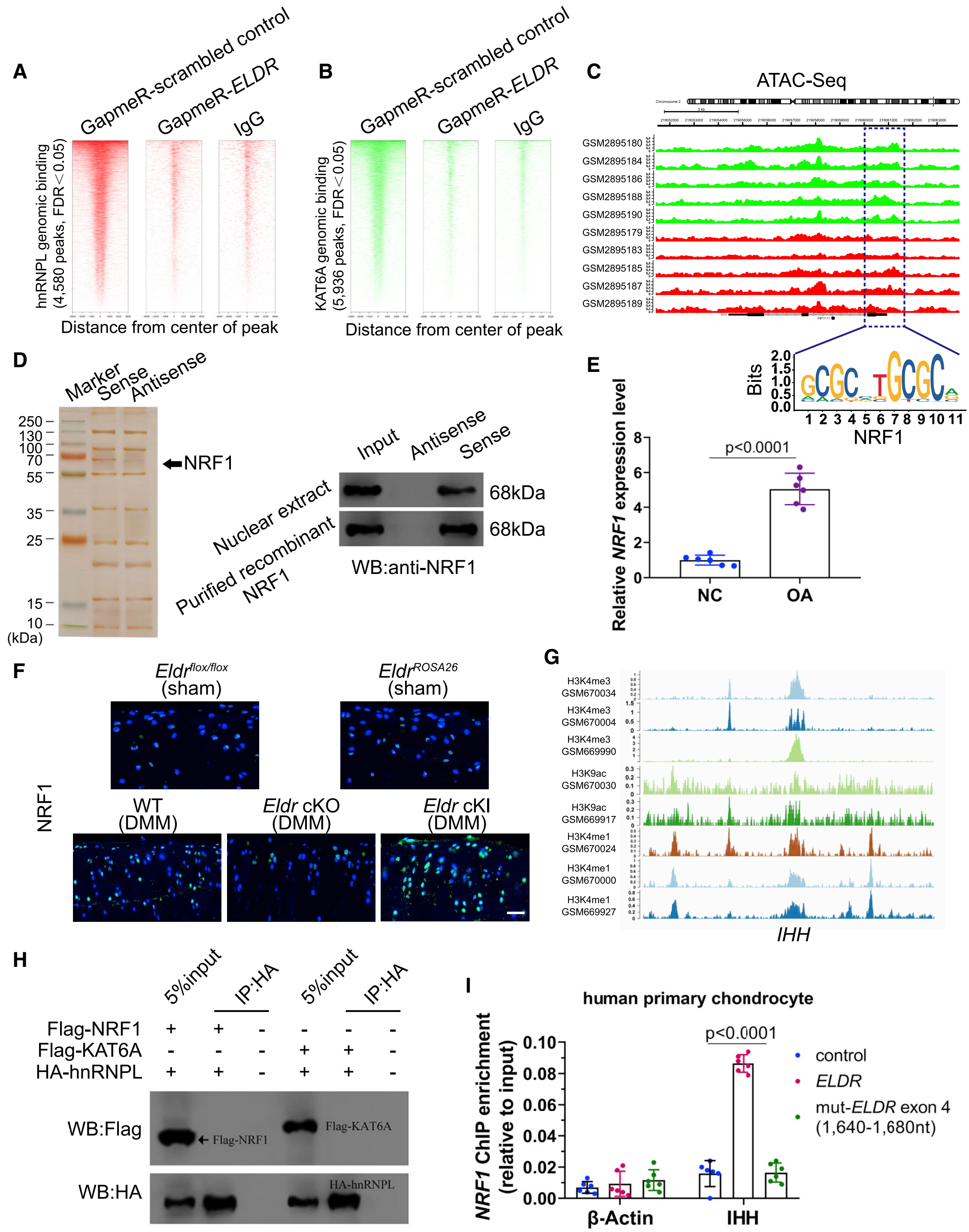

Figure 6. *ELDR*/hnRNPL/KAT6A creates an open chromatin region in the *IHH* promoter for NRF1 binding
(A) The binding sites of hnRNPL in global genome through analysis of gene expression in chondrocytes after transfection of GapmeR-*ELDR*.
(B) The binding sites of KAT6A in global genome through analysis of gene expression in chondrocytes after transfection of GapmeR-*ELDR*.
(C) ATAC-seq analysis showing accessible chromatin region in *IHH* promoter in OA-affected individuals and motif enrichment analysis reveals a transcription factor (NRF1) relevant to OA.
(D) The transcription factor was further confirmed by DNA pull-down and immunoblot.
(E) RT-qPCR analysis of *NRF1* expression in human primary chondrocytes from OA and controls. n = 6 biological replicates per group.
(F) Immunostaining of NRF1 in cartilage tissues of the above-mentioned groups. n = 6 mice per group.
(G) ChIP-seq analysis demonstrating the enrichment of H3K4me3, H3K9ac, and H3K4me1 in *IHH* promoter region.
(H) Co-IP analysis showing the relationships between NRF1 and hnRNPL or KAT6A in chondrocytes.

(legend continued on next page)

by *ELDR* overexpression (Figure S5M). However, downregulation of *IHH* caused by *ELDR* silencing can be partially restored by *hnRNPL* or *KAT6A* overexpression (Figure S5M). Taken together, these data imply that *ELDR* regulates *IHH* expression through hnRNPL- and KAT6A-mediated methylation of H3K4 and acetylation of H3K9, respectively.

ELDR/hnRNPL/KAT6A complex facilitates the binding between NRF1 and the *IHH* promoter sequence

Dynamic changes at specific chromosomal loci have been demonstrated to expose protein-binding sites, thereby allowing the recruitment of *trans*-factors and resulting in the alteration of gene transcription.[61] To address whether *ELDR* modulates hnRNPL and KAT6A genomic binding genome wide, we performed ChIP-seq for hnRNPL and KAT6A in chondrocytes. The ChIP-seq data (hnRNPL and KAT6A) showed 4,580 and 5,936 called peaks, respectively, in chondrocytes transfected with GapmeR-scrambled control. GapmeR-*ELDR* caused reduced hnRNPL and KAT6A occupancies in these two histone-modulator-binding DNA regions (Figures 6A and 6B). A substantial subset of genes that exhibit decreased binding by the hnRNPL/KAT6A complex was dysregulated after knockdown of *ELDR* (Figure S6A). Integrative GSEA of the RNA-seq and hnRNPL/KAT6A ChIP-seq data revealed significant enrichment for genes that were downregulated when *ELDR* was silenced (Figure S6B). Furthermore, we comprehensively analyzed ATAC-seq data of human OA chondrocytes deposited in Cistrome Data Browser and found that an open chromatin status was present in chromosomal region chr2q35. This region encodes the protein-coding gene *IHH*. Importantly, the open chromatin status triggers recruitment of the transcription factor NRF1 at the promoter of *IHH* (Figure 6C), an important transcription factor in OA pathogenesis.[62,63] With DNA pull-down and mass spectrometry analysis, one band was identified as NRF1 (Figures 6D and S6C). Furthermore, the *NRF1* expression level was determined in chondrocytes and cartilage tissues from human and mice OA (Figures 6E, 6F, and S6D). Given the critical role of histone modification in dynamic chromatin tuning,[64,65] we analyzed the profiles of histone methylation and acetylation in *IHH* promoter by using ChIP-seq data (GSM670034, GSM670004, GSM669990, GSM670030, and GSM669917). The result showed peak enrichment in H3K4me3, H3K9ac, and H3K4me1 marks in the *IHH* promoter (Figure 6G). Using human OA and control chondrocytes, we further confirmed this result in our ChIP-qPCR study (Figure S6E).

To further study the formation of the *ELDR*/transcription factor/epigenetic modulator complex, we performed co-immunoprecipitation (co-IP) by using hemagglutinin (HA)-tagged beads and found that NRF1 did not directly interact with hnRNPL or KAT6A (Figure 6H), whereas the results of the RNA pull-down assay showed that *ELDR* could interact with both hnRNPL and KAT6A. The ChIP analysis revealed that NRF1 could interact with the *IHH* promoter and that this interaction was dependent on high expression of *ELDR* (Figures 6I and S6F). However, the interaction between NRF1 and the *IHH* promoter was not detected in chondrocytes overexpressing *ELDR* while hnRNPL and KAT6A were knocked down (Figure S6G). In contrast, the binding between NRF1 and the *IHH* promoter was not observed in *ELDR* knockdown, although overexpressing *hnRNPL* and *KAT6A* (Figure S6G). These data indicate that open chromatin status in the *IHH* promoter induced by the *ELDR*/hnRNPL/KAT6A complex provides a unique opportunity for NRF1 binding onto the *IHH* promoter, initiating *IHH* expression and chondrocyte senescence. Therefore, our findings form the basis for the exploration of chromatin dynamics biology and provide potential targets for the diagnosis and treatment of OA.

Therapeutic potential of *Eldr* in chondrocyte senescence and OA

Eliminating senescent cells and attenuating the SASP have emerged as attractive therapeutic strategies.[54] We therefore sought to investigate the therapeutic role of *Eldr* in OA and to elucidate the underlying molecular mechanisms involved. An OA model was induced in WT mice, followed by local injection of GapmeR-*Eldr* or GapmeR-scrambled control at 7, 14, and 21 days after surgery (Figure 7A). The ability of the GapmeR to target cartilage *in vivo* was monitored in real time (Figure S7A). Furthermore, Cy3-labeled GapmeR-*Eldr* analysis showed that *Eldr* could penetrate cartilage (Figure S7B). Local delivery of GapmeR-*Eldr* remarkably protected the structure of cartilage as determined by gross appearance (Figure 7B), histological assessments (Figures 7B, S7C, and S7D), and radiography (Figures 7C, S7E, and S7F), indicating that silencing of *Eldr* had a protective effect against surgically induced OA. Conversely, mice treated with GapmeR-scrambled control developed severe osteoarthritic phenotype (Figures 7B and 7C). At a molecular level, *Eldr* knockdown in knee joints of DMM-operated mice attenuated Ihh signaling (Figures 7D and S7G), thereby inhibiting both inflammatory SASP factors and cellular senescence in cartilage (Figures 7E and S7H). Compared with PBS and GapmeR-scrambled control groups, telomere maintenance was observed in the GapmeR-*Eldr* treating group (Figure 7F), suggesting that *Eldr* promotes telomeric loss and causes premature aging. In addition, chondrocyte proliferation was investigated by the EdU analysis (Figure S7I), implying that knockdown of *Eldr* remarkably promotes chondrocyte proliferation. In pain-related behavioral tests, mice receiving GapmeR-*Eldr* injection exhibited higher pain thresholds (Figure S7J), indicating that silencing of *Eldr* in OA knee joints not only ameliorates histological

(I) ChIP-qPCR analysis of the NRF1 genomic occupancy in *IHH* promoter after overexpression or site-directed mutagenesis of *EDLR* in human primary chondrocytes. n = 6 biological replicates per group. Scale bar: 20 μm (F). All graphs are presented as the mean ± SEM. p values are from unpaired t test with Welch's correction (E) and one-way ANOVA followed by Tukey's post hoc (I).

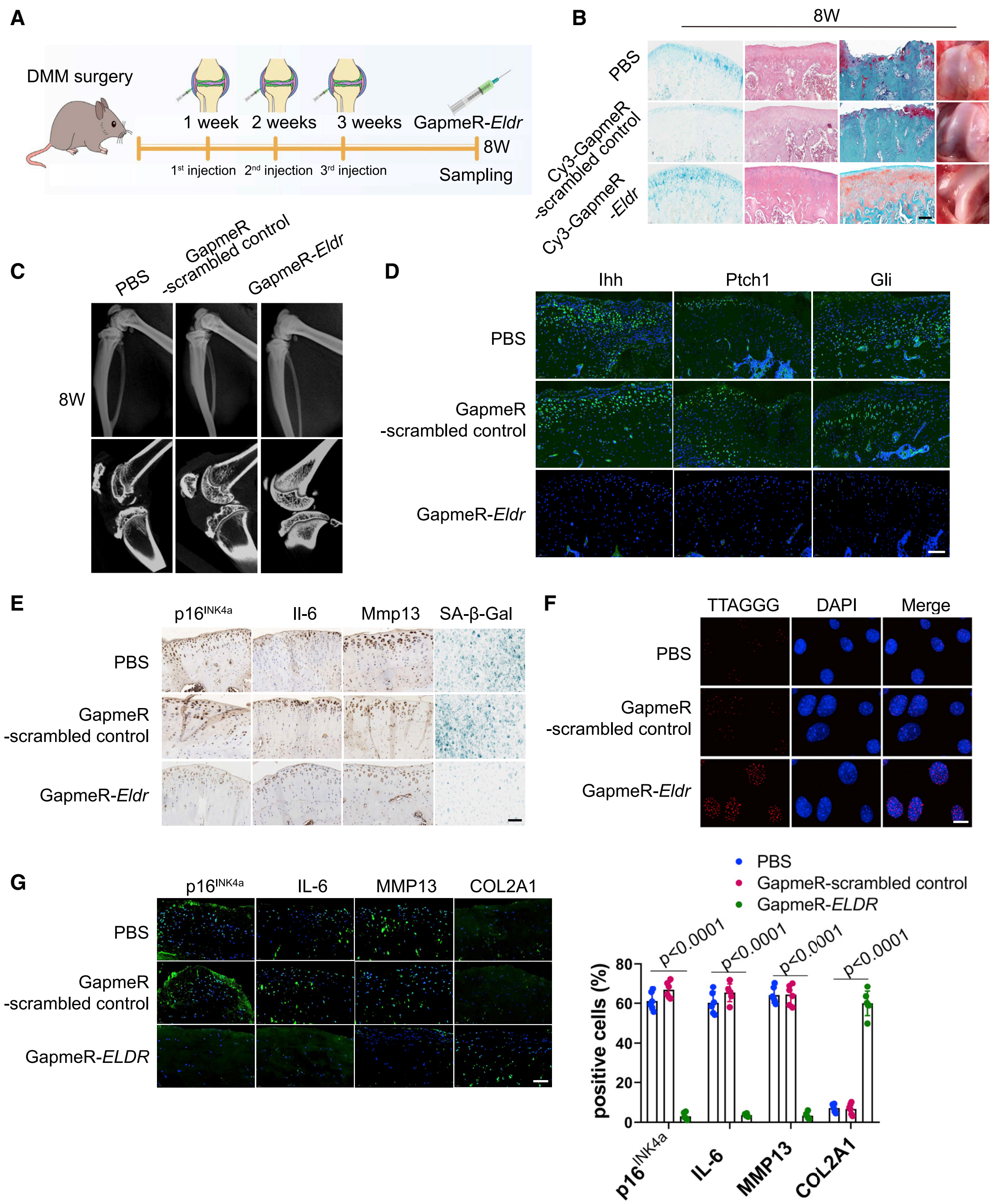

Figure 7. Pharmacological inhibition of *ELDR in vivo* attenuates chondrocyte senescence and cartilage degradation

(A) The treatment strategy for examining the effect of GapmeR-*Eldr* on OA progression.

(B) The cartilage degradation evaluated by Alcian blue, H&E, and safranin-O staining and gross appearance. n = 6 mice per group.

(C) X-ray and micro-CT in WT mice subjected to DMM surgery followed by treatment with PBS, GapmeR-scrambled control, and GapmeR-*Eldr* at indicated weeks. n = 6 mice per group.

(D) Ptch1 and Gli are the downstream genes of Ihh signaling. Determining their levels in cartilage can further confirm the essential role of Ihh signaling in OA. Representative images of immunostaining of Ihh, Ptch1, and Gli in cartilage from the indicated groups of mice. n = 6 mice per group.

(E) Representative images of immunohistochemistry of $p16^{INK4a}$, Il-6, and Mmp13 localization in cartilage and SA-β-Gal staining in chondrocytes from mice treated with PBS, GapmeR-scrambled control, and GapmeR-*Eldr*, respectively. n = 6 mice per group.

(F) Representative fluorescence microscopy images of telomere FISH analysis in chondrocytes from mice undergoing PBS, GapmeR-scrambled control, or GapmeR-*Eldr* treatment. n = 6 mice per group.

(G) Representative images of immunostaining of $p16^{INK4a}$, IL-6, MMP13, and COL2A1 in human OA cartilage treated with PBS, GapmeR-scrambled control, or GapmeR-*ELDR*. n = 6 biological replicates per group. Scale bar: 10 μm (F), 50 μm (B, E, and G), and 100 μm (D). All graphs are presented as the mean ± SEM. p values are from one-way ANOVA test followed by Tukey's post hoc (MMP13 level in G) and Brown-Forsythe and Welch ANOVA test followed by Tamhane's T2 post hoc ($p16^{INK4a}$, IL-6, and COL2A1 levels in G).

features but also reduces pain, a prominent symptom affecting individuals with OA.

Intriguingly, to test the feasibility of *ELDR*-targeting therapy in clinical OA, we evaluated the effect of *ELDR* antagonism in an explant culture of cartilage from OA-affected individuals undergoing total knee arthroplasty. *ELDR* inhibition in OA-affected tissue explants augmented the amount of anabolic markers and suppressed the expression of senescence markers and catabolic mediators (Figures 7G, S7K, and S7L). Moreover, TUNEL staining showed remarkably decreased chondrocyte apoptosis in cartilage explants treated with GapmeR-*ELDR* (Figure S7M). Collectively, these data demonstrate that therapeutic targeting of *ELDR* could elicit clinically desirable effects.

Discussion

The present study elucidated the pivotal role of *ELDR* in chondrocyte senescence and cartilage degradation, adding support for how dysregulated *ELDR* can drive distinct senescent phenotypes *in vivo*. The data from mice and human studies indicate increased activation of hedgehog signaling in OA and that the use of hedgehog signaling inhibitors could attenuate the severity of OA or even prevent its development.[55,66] Furthermore, aberrantly high IHH signaling has previously been shown to promote aging.[67,68] Importantly, our results reveal that local intra-articular administration of GapmeR-*Eldr* in mice substantially inhibits chondrocyte senescence and SASP by silencing hedgehog signaling. Similar results were also found in human osteoarthritic cartilage explants. These findings provide in-depth mechanistic and translational insights into the hedgehog pathway and could ultimately develop senolytic therapy for age-associated and post-traumatic OA treatment, moving beyond symptomatic relief to disease-modifying OA drugs.

Similar to pre-mRNA, noncoding exons in lncRNAs also undergo alternative splicing, a ubiquitous regulatory mechanism of gene expression, to produce different isoforms, which have specific expression patterns in human diseases.[69,70] Furthermore, unlike protein-coding exons, almost all noncoding exons were found to be alternatively spliced, indicating that splicing patterns in lncRNAs may be different from those in protein-coding genes.[71] In this study, a novel transcript of *ELDR* (2,724 nt) formed by exons 1, 3, and 4 was identified in human chondrocytes, whereas two transcripts of *ELDR* included in public databases, 470 nt (NR_110426.1) and 2,941 nt (ENST00000626532.1), were not detected in our experiment. These findings indicate that this novel transcript may be required for human chondrocyte in the context of physiologically normal and OA states. The molecular mechanisms underlying *ELDR* alternative splicing in human chondrocytes should be extensively investigated in future studies, probably offering hope for combating OA with splicing modulation.

Unlike transcription factors, hnRNPL and KAT6A proteins lack putative DNA-binding motifs, so the mechanisms by which hnRNPL and KAT6A orient themself to their target sites across the chromatin remain unclear. The potential of RNA to bind to complementary DNA sequences has led to the hypothesis that lncRNAs could play crucial guiding roles in the establishment and transmission of chromatin states.[21,59] In our study, *ELDR* can act as a scaffold to bring hnRNPL and KAT6A proteins to specific histone modifications loci of the *IHH* promoter through the formation of an RNA-DNA triplex. This finding further explains why chromatin-modifying complexes can bind to numerous gene promoters in a sequence-specific manner with limited binding domains.

Cellular senescence, a process that imposes permanent proliferative arrest on cells in response to various stressors, is a largely epigenetically determined cellular event.[14,72] It should be noted that lncRNAs have emerged in recent years as key epigenetic regulators of diverse cellular processes and can regulate gene expression in *cis* or in *trans*.[22,59] The central finding of our study is that epigenetic modifiers and transcription factors co-regulate the hedgehog signaling pathway involved in chondrocyte senescence in the context of high levels of *ELDR*. Histone modifications are frequently enriched at distinct genomic locations and particularly at genes, where their presence is positively or negatively correlated with transcriptional activity.[65] H3K4me3 and H3K9ac enable the recruitment of transcriptional machinery and thus potentially facilitates transcription.[73,74] Our mechanistic study shows that exon 4 of *ELDR* recruits hnRNPL and KAT6A to the histones of the *IHH* promoter region and increases H3K4me3 and H3K9ac levels. It creates an open chromatin region in the *IHH* promoter,[75,76] enabling NRF1 to bind and thus modulating hedgehog signaling. These findings imply that *ELDR* determines the specific interaction of hnRNPL and KAT6A as a multi-protein-modified complex to execute a unique transcriptional regulatory role of NRF1 in the regulation of hedgehog signaling, highlighting the highly dynamic nature of the epigenome during OA.[7] Targeting the epigenetic alterations observed in senescent cells holds great therapeutic prospects because of the reversible nature of epigenetic mechanisms.[77,78] The importance of the aberrant chromatin state of senescent chondrocytes will therefore give an impetus for the clinical development of epigenetic therapies aimed at resetting the histone modifications imbalance observed in OA.

In summary, our study reveals an epigenetic switch for transcriptome reprogramming in chondrocyte senescence and cartilage degradation. The discovery of a lncRNA-mediated regulatory axis in aging and injury-induced chondrocyte senescence could shed light on the complex interactions between epigenetic modifiers and transcription factors. Therefore, synthetically engineered *ELDR* containing the functional domains that act on the active regions of hedgehog signaling proteins can be tested for their therapeutic effects on OA. This could offer opportunities to develop RNA-based senolytic agents in a cell-type-specific manner, representing a new paradigm for OA therapy.

Data and code availability

The microarray and sequencing data generated during this study are available in GEO under the accession code GEO: GSE174049, GSE178090, GSE178091, and GSE178092 (https://www.ncbi.nlm.nih.gov/geo/query/acc.cgi?acc=GSE178092). Any remaining data that support the results of the study are available from the corresponding author upon reasonable request.

Supplemental information

Supplemental information can be found online at https://doi.org/10.1016/j.ajhg.2023.02.011.

Acknowledgments

This work is supported by The National Natural Science Foundation of China (no. 81972105, no. 82272557, no. 82072427, and no. 81672159), and the Fundamental Research Funds for the Central Universities (no. 2242019K3DZ05).

Declaration of interests

The authors declare no competing interests.

Received: October 11, 2022
Accepted: February 10, 2023
Published: March 2, 2023

Web resources

Cistrome Data Browser, http://cistrome.org/db/#/
CRISPR design tool, http://www.sanger.ac.uk/htgt/wge/
Ensembl genome brower, http://asia.ensembl.org/index.html
LNCipedia, https://lncipedia.org/
NCBI, https://pubmed.ncbi.nlm.nih.gov/
Stellaris RNA FISH, https://www.biosearchtech.com/support/education/stellaris-rna-fish
UCSC genome browser, http://genome.ucsc.edu/
UniProtKB, https://www.uniprot.org/

References

1. Loeser, R.F., Collins, J.A., and Diekman, B.O. (2016). Ageing and the pathogenesis of osteoarthritis. Nat. Rev. Rheumatol. *12*, 412–420.
2. Jeon, O.H., Kim, C., Laberge, R.M., Demaria, M., Rathod, S., Vasserot, A.P., Chung, J.W., Kim, D.H., Poon, Y., David, N., et al. (2017). Local clearance of senescent cells attenuates the development of post-traumatic osteoarthritis and creates a pro-regenerative environment. Nat. Med. *23*, 775–781.
3. McCulloch, K., Litherland, G.J., and Rai, T.S. (2017). Cellular senescence in osteoarthritis pathology. Aging Cell *16*, 210–218.
4. Gorgoulis, V., Adams, P.D., Alimonti, A., Bennett, D.C., Bischof, O., Bishop, C., Campisi, J., Collado, M., Evangelou, K., Ferbeyre, G., et al. (2019). Cellular senescence: defining a path forward. Cell *179*, 813–827.
5. Choi, W.S., Lee, G., Song, W.H., Koh, J.T., Yang, J., Kwak, J.S., Kim, H.E., Kim, S.K., Son, Y.O., Nam, H., et al. (2019). The CH25H-CYP7B1-RORalpha axis of cholesterol metabolism regulates osteoarthritis. Nature *566*, 254–258.
6. Martel-Pelletier, J., Barr, A.J., Cicuttini, F.M., Conaghan, P.G., Cooper, C., Goldring, M.B., Goldring, S.R., Jones, G., Teichtahl, A.J., and Pelletier, J.P. (2016). Osteoarthritis. Nat. Rev. Dis. Primers *2*, 16072.
7. Richard, D., Liu, Z., Cao, J., Kiapour, A.M., Willen, J., Yarlagadda, S., Jagoda, E., Kolachalama, V.B., Sieker, J.T., Chang, G.H., et al. (2020). Evolutionary selection and constraint on human knee chondrocyte regulation impacts osteoarthritis risk. Cell *181*, 362–381.e28.
8. Wallace, I.J., Worthington, S., Felson, D.T., Jurmain, R.D., Wren, K.T., Maijanen, H., Woods, R.J., and Lieberman, D.E. (2017). Knee osteoarthritis has doubled in prevalence since the mid-20th century. Proc. Natl. Acad. Sci. USA *114*, 9332–9336.
9. Jeon, O.H., David, N., Campisi, J., and Elisseeff, J.H. (2018). Senescent cells and osteoarthritis: a painful connection. J. Clin. Invest. *128*, 1229–1237.
10. He, S., and Sharpless, N.E. (2017). Senescence in health and disease. Cell *169*, 1000–1011.
11. Mokuda, S., Nakamichi, R., Matsuzaki, T., Ito, Y., Sato, T., Miyata, K., Inui, M., Olmer, M., Sugiyama, E., Lotz, M., and Asahara, H. (2019). Wwp2 maintains cartilage homeostasis through regulation of Adamts5. Nat. Commun. *10*, 2429.
12. Matsuzaki, T., Alvarez-Garcia, O., Mokuda, S., Nagira, K., Olmer, M., Gamini, R., Miyata, K., Akasaki, Y., Su, A.I., Asahara, H., and Lotz, M.K. (2018). FoxO transcription factors modulate autophagy and proteoglycan 4 in cartilage homeostasis and osteoarthritis. Sci. Transl. Med. *10*, eaan0746.
13. Ji, Q., Zheng, Y., Zhang, G., Hu, Y., Fan, X., Hou, Y., Wen, L., Li, L., Xu, Y., Wang, Y., and Tang, F. (2019). Single-cell RNA-seq analysis reveals the progression of human osteoarthritis. Ann. Rheum. Dis. *78*, 100–110.
14. Jeon, O.H., Wilson, D.R., Clement, C.C., Rathod, S., Cherry, C., Powell, B., Lee, Z., Khalil, A.M., Green, J.J., Campisi, J., et al. (2019). Senescence cell-associated extracellular vesicles serve as osteoarthritis disease and therapeutic markers. JCI Insight *4*, e125019.
15. Batshon, G., Elayyan, J., Qiq, O., Reich, E., Ben-Aderet, L., Kandel, L., Haze, A., Steinmeyer, J., Lefebvre, V., Zhang, H., et al. (2020). Serum NT/CT SIRT1 ratio reflects early osteoarthritis and chondrosenescence. Ann. Rheum. Dis. *79*, 1370–1380.
16. Martínez-Zamudio, R.I., Roux, P.F., de Freitas, J., Robinson, L., Doré, G., Sun, B., Belenki, D., Milanovic, M., Herbig, U., Schmitt, C.A., et al. (2020). AP-1 imprints a reversible transcriptional programme of senescent cells. Nat. Cell Biol. *22*, 842–855.
17. Partridge, L., Fuentealba, M., and Kennedy, B.K. (2020). The quest to slow ageing through drug discovery. Nat. Rev. Drug Discov. *19*, 513–532.
18. Pignolo, R.J., Passos, J.F., Khosla, S., Tchkonia, T., and Kirkland, J.L. (2020). Reducing senescent cell burden in aging and disease. Trends Mol. Med. *26*, 630–638.
19. Andergassen, D., and Rinn, J.L. (2022). From genotype to phenotype: genetics of mammalian long non-coding RNAs in vivo. Nat. Rev. Genet. *23*, 229–243.
20. Nojima, T., and Proudfoot, N.J. (2022). Mechanisms of lncRNA biogenesis as revealed by nascent transcriptomics. Nat. Rev. Mol. Cell Biol. *23*, 389–406.
21. Batista, P.J., and Chang, H.Y. (2013). Long noncoding RNAs: cellular address codes in development and disease. Cell *152*, 1298–1307.
22. Hung, T., Wang, Y., Lin, M.F., Koegel, A.K., Kotake, Y., Grant, G.D., Horlings, H.M., Shah, N., Umbricht, C., Wang, P., et al.

(2011). Extensive and coordinated transcription of noncoding RNAs within cell-cycle promoters. Nat. Genet. *43*, 621–629.
23. Rinn, J.L., Kertesz, M., Wang, J.K., Squazzo, S.L., Xu, X., Brugmann, S.A., Goodnough, L.H., Helms, J.A., Farnham, P.J., Segal, E., and Chang, H.Y. (2007). Functional demarcation of active and silent chromatin domains in human HOX loci by noncoding RNAs. Cell *129*, 1311–1323.
24. Pandey, R.R., Mondal, T., Mohammad, F., Enroth, S., Redrup, L., Komorowski, J., Nagano, T., Mancini-Dinardo, D., and Kanduri, C. (2008). Kcnq1ot1 antisense noncoding RNA mediates lineage-specific transcriptional silencing through chromatin-level regulation. Mol. Cell *32*, 232–246.
25. Li, L., van Breugel, P.C., Loayza-Puch, F., Ugalde, A.P., Korkmaz, G., Messika-Gold, N., Han, R., Lopes, R., Barbera, E.P., Teunissen, H., et al. (2018). LncRNA-OIS1 regulates DPP4 activation to modulate senescence induced by RAS. Nucleic Acids Res. *46*, 4213–4227.
26. Kumar, P.P., Emechebe, U., Smith, R., Franklin, S., Moore, B., Yandell, M., Lessnick, S.L., and Moon, A.M. (2014). Coordinated control of senescence by lncRNA and a novel T-box3 co-repressor complex. Elife *3*, e02805.
27. Mondal, T., Subhash, S., Vaid, R., Enroth, S., Uday, S., Reinius, B., Mitra, S., Mohammed, A., James, A.R., Hoberg, E., et al. (2015). MEG3 long noncoding RNA regulates the TGF-β pathway genes through formation of RNA-DNA triplex structures. Nat. Commun. *6*, 7743.
28. Kuo, C.C., Hänzelmann, S., Sentürk Cetin, N., Frank, S., Zajzon, B., Derks, J.P., Akhade, V.S., Ahuja, G., Kanduri, C., Grummt, I., et al. (2019). Detection of RNA-DNA binding sites in long noncoding RNAs. Nucleic Acids Res. *47*, e32.
29. Pearson, M.J., Philp, A.M., Heward, J.A., Roux, B.T., Walsh, D.A., Davis, E.T., Lindsay, M.A., and Jones, S.W. (2016). Long intergenic noncoding RNAs mediate the human chondrocyte inflammatory response and are differentially expressed in osteoarthritis cartilage. Arthritis Rheumatol. *68*, 845–856.
30. Liu, Q., Zhang, X., Dai, L., Hu, X., Zhu, J., Li, L., Zhou, C., and Ao, Y. (2014). Long noncoding RNA related to cartilage injury promotes chondrocyte extracellular matrix degradation in osteoarthritis. Arthritis Rheumatol. *66*, 969–978.
31. Fu, M., Huang, G., Zhang, Z., Liu, J., Zhang, Z., Huang, Z., Yu, B., and Meng, F. (2015). Expression profile of long noncoding RNAs in cartilage from knee osteoarthritis patients. Osteoarthritis Cartilage *23*, 423–432.
32. Yamasaki, K., Nakasa, T., Miyaki, S., Ishikawa, M., Deie, M., Adachi, N., Yasunaga, Y., Asahara, H., and Ochi, M. (2009). Expression of MicroRNA-146a in osteoarthritis cartilage. Arthritis Rheum. *60*, 1035–1041.
33. Wu, J., Mao, X., Cai, T., Luo, J., and Wei, L. (2006). KOBAS server: a web-based platform for automated annotation and pathway identification. Nucleic Acids Res. *34*, W720–W724. Web Server issue.
34. Bellaousov, S., Reuter, J.S., Seetin, M.G., and Mathews, D.H. (2013). RNAstructure: Web servers for RNA secondary structure prediction and analysis. Nucleic Acids Res. *41*, W471–W474. Web Server issue.
35. He, S., Zhang, H., Liu, H., and Zhu, H. (2015). LongTarget: a tool to predict lncRNA DNA-binding motifs and binding sites via Hoogsteen base-pairing analysis. Bioinformatics *31*, 178–186.
36. Amin, F., Ibrahim, M.A.A., Rizwan-Ul-Hasan, S., Khaliq, S., Gabr, G.A., Muhammad, K.A., Khan, A., Sidhom, P.A., Tikmani, P., Shawky, A.M., et al. (2022). Interactions of apigenin and safranal with the 5HT1A and 5HT2A receptors and behavioral effects in depression and anxiety: a molecular docking, lipid-mediated molecular dynamics, and in vivo analysis. Molecules *27*, 8658.
37. Rackers, J.A., Liu, C., Ren, P., and Ponder, J.W. (2018). A physically grounded damped dispersion model with particle mesh Ewald summation. J. Chem. Phys. *149*, 084115.
38. Morzan, U.N., Ramírez, F.F., Oviedo, M.B., Sánchez, C.G., Scherlis, D.A., and Lebrero, M.C.G. (2014). Electron dynamics in complex environments with real-time time dependent density functional theory in a QM-MM framework. J. Chem. Phys. *140*, 164105.
39. Son, Y.O., Park, S., Kwak, J.S., Won, Y., Choi, W.S., Rhee, J., Chun, C.H., Ryu, J.H., Kim, D.K., Choi, H.S., and Chun, J.S. (2017). Estrogen-related receptor gamma causes osteoarthritis by upregulating extracellular matrix-degrading enzymes. Nat. Commun. *8*, 2133.
40. Rhee, J., Park, S.H., Kim, S.K., Kim, J.H., Ha, C.W., Chun, C.H., and Chun, J.S. (2017). Inhibition of BATF/JUN transcriptional activity protects against osteoarthritic cartilage destruction. Ann. Rheum. Dis. *76*, 427–434.
41. Wei, Y., Luo, L., Gui, T., Yu, F., Yan, L., Yao, L., Zhong, L., Yu, W., Han, B., Patel, J.M., et al. (2021). Targeting cartilage EGFR pathway for osteoarthritis treatment. Sci. Transl. Med. *13*, eabb3946.
42. Huang, J., Zhao, L., Fan, Y., Liao, L., Ma, P.X., Xiao, G., and Chen, D. (2019). The microRNAs miR-204 and miR-211 maintain joint homeostasis and protect against osteoarthritis progression. Nat. Commun. *10*, 2876.
43. Xiao, B., Wang, Y., Li, W., Baker, M., Guo, J., Corbet, K., Tsalik, E.L., Li, Q.J., Palmer, S.M., Woods, C.W., et al. (2013). Plasma microRNA signature as a noninvasive biomarker for acute graft-versus-host disease. Blood *122*, 3365–3375.
44. Ji, M.L., Jiang, H., Zhang, X.J., Shi, P.L., Li, C., Wu, H., Wu, X.T., Wang, Y.T., Wang, C., and Lu, J. (2018). Preclinical development of a microRNA-based therapy for intervertebral disc degeneration. Nat. Commun. *9*, 5051.
45. Ji, M.L., Jiang, H., Wu, F., Geng, R., Ya, L.K., Lin, Y.C., Xu, J.H., Wu, X.T., and Lu, J. (2021). Precise targeting of miR-141/200c cluster in chondrocytes attenuates osteoarthritis development. Ann. Rheum. Dis. *80*, 356–366.
46. Ransohoff, J.D., Wei, Y., and Khavari, P.A. (2018). The functions and unique features of long intergenic non-coding RNA. Nat. Rev. Mol. Cell Biol. *19*, 143–157.
47. Uszczynska-Ratajczak, B., Lagarde, J., Frankish, A., Guigó, R., and Johnson, R. (2018). Towards a complete map of the human long non-coding RNA transcriptome. Nat. Rev. Genet. *19*, 535–548.
48. Karro, J.E., Yan, Y., Zheng, D., Zhang, Z., Carriero, N., Cayting, P., Harrison, P., and Gerstein, M. (2007). Pseudogene.org: a comprehensive database and comparison platform for pseudogene annotation. Nucleic Acids Res. *35*, D55–D60.
49. Singer, R.A., Arnes, L., Cui, Y., Wang, J., Gao, Y., Guney, M.A., Burnum-Johnson, K.E., Rabadan, R., Ansong, C., Orr, G., and Sussel, L. (2019). The long noncoding RNA paupar modulates PAX6 regulatory activities to promote alpha cell development and function. Cell Metab. *30*, 1091–1106.e8.
50. Kong, L., Zhang, Y., Ye, Z.Q., Liu, X.Q., Zhao, S.Q., Wei, L., and Gao, G. (2007). CPC: assess the protein-coding potential of transcripts using sequence features and support vector machine. Nucleic Acids Res. *35*, W345–W349. Web Server issue.

51. Wang, L., Park, H.J., Dasari, S., Wang, S., Kocher, J.P., and Li, W. (2013). CPAT: coding-potential assessment tool using an alignment-free logistic regression model. Nucleic Acids Res. *41*, e74.
52. Storer, M., Mas, A., Robert-Moreno, A., Pecoraro, M., Ortells, M.C., Di Giacomo, V., Yosef, R., Pilpel, N., Krizhanovsky, V., Sharpe, J., and Keyes, W.M. (2013). Senescence is a developmental mechanism that contributes to embryonic growth and patterning. Cell *155*, 1119–1130.
53. Muñoz-Espín, D., and Serrano, M. (2014). Cellular senescence: from physiology to pathology. Nat. Rev. Mol. Cell Biol. *15*, 482–496.
54. Faust, H.J., Zhang, H., Han, J., Wolf, M.T., Jeon, O.H., Sadtler, K., Peña, A.N., Chung, L., Maestas, D.R., Jr., Tam, A.J., et al. (2020). IL-17 and immunologically induced senescence regulate response to injury in osteoarthritis. J. Clin. Invest. *130*, 5493–5507.
55. Lin, A.C., Seeto, B.L., Bartoszko, J.M., Khoury, M.A., Whetstone, H., Ho, L., Hsu, C., Ali, S.A., and Alman, B.A. (2009). Modulating hedgehog signaling can attenuate the severity of osteoarthritis. Nat. Med. *15*, 1421–1425.
56. Song, E.K., Jeon, J., Jang, D.G., Kim, H.E., Sim, H.J., Kwon, K.Y., Medina-Ruiz, S., Jang, H.J., Lee, A.R., Rho, J.G., et al. (2018). ITGBL1 modulates integrin activity to promote cartilage formation and protect against arthritis. Sci. Transl. Med. *10*, eaam7486.
57. Son, Y.O., Kim, H.E., Choi, W.S., Chun, C.H., and Chun, J.S. (2019). RNA-binding protein ZFP36L1 regulates osteoarthritis by modulating members of the heat shock protein 70 family. Nat. Commun. *10*, 77.
58. Yao, R.W., Wang, Y., and Chen, L.L. (2019). Cellular functions of long noncoding RNAs. Nat. Cell Biol. *21*, 542–551.
59. Fatica, A., and Bozzoni, I. (2014). Long non-coding RNAs: new players in cell differentiation and development. Nat. Rev. Genet. *15*, 7–21.
60. Baell, J.B., Leaver, D.J., Hermans, S.J., Kelly, G.L., Brennan, M.S., Downer, N.L., Nguyen, N., Wichmann, J., McRae, H.M., Yang, Y., et al. (2018). Inhibitors of histone acetyltransferases KAT6A/B induce senescence and arrest tumour growth. Nature *560*, 253–257.
61. Price, B.D., and D'Andrea, A.D. (2013). Chromatin remodeling at DNA double-strand breaks. Cell *152*, 1344–1354.
62. Bartelt, A., Widenmaier, S.B., Schlein, C., Johann, K., Goncalves, R.L.S., Eguchi, K., Fischer, A.W., Parlakgül, G., Snyder, N.A., Nguyen, T.B., et al. (2018). Brown adipose tissue thermogenic adaptation requires Nrf1-mediated proteasomal activity. Nat. Med. *24*, 292–303.
63. Wang, Y., Zhao, X., Lotz, M., Terkeltaub, R., and Liu-Bryan, R. (2015). Mitochondrial biogenesis is impaired in osteoarthritis chondrocytes but reversible via peroxisome proliferator-activated receptor γ coactivator 1α. Arthritis Rheumatol. *67*, 2141–2153.
64. Kan, R.L., Chen, J., and Sallam, T. (2022). Crosstalk between epitranscriptomic and epigenetic mechanisms in gene regulation. Trends Genet. *38*, 182–193.
65. Millán-Zambrano, G., Burton, A., Bannister, A.J., and Schneider, R. (2022). Histone post-translational modifications - cause and consequence of genome function. Nat. Rev. Genet. *23*, 563–580.
66. Alman, B.A. (2015). The role of hedgehog signalling in skeletal health and disease. Nat. Rev. Rheumatol. *11*, 552–560.
67. Scheffold, A., Baig, A.H., Chen, Z., von Löhneysen, S.E., Becker, F., Morita, Y., Avila, A.I., Groth, M., Lechel, A., Schmid, F., et al. (2020). Elevated Hedgehog activity contributes to attenuated DNA damage responses in aged hematopoietic cells. Leukemia *34*, 1125–1134.
68. Templeman, N.M., Cota, V., Keyes, W., Kaletsky, R., and Murphy, C.T. (2020). CREB non-autonomously controls reproductive aging through hedgehog/patched signaling. Dev. Cell *54*, 92–105.e5.
69. Wang, Z., Yang, B., Zhang, M., Guo, W., Wu, Z., Wang, Y., Jia, L., Li, S., Cancer Genome Atlas Research Network, Xie, W., and Yang, D. (2018). lncRNA epigenetic landscape analysis identifies EPIC1 as an oncogenic lncRNA that interacts with MYC and promotes cell-cycle progression in cancer. Cancer Cell *33*, 706–720.e9.
70. Zhou, H.Z., Li, F., Cheng, S.T., Xu, Y., Deng, H.J., Gu, D.Y., Wang, J., Chen, W.X., Zhou, Y.J., Yang, M.L., et al. (2022). DDX17-regulated alternative splicing that produced an oncogenic isoform of PXN-AS1 to promote HCC metastasis. Hepatology *75*, 847–865.
71. Tilgner, H., Jahanbani, F., Blauwkamp, T., Moshrefi, A., Jaeger, E., Chen, F., Harel, I., Bustamante, C.D., Rasmussen, M., and Snyder, M.P. (2015). Comprehensive transcriptome analysis using synthetic long-read sequencing reveals molecular co-association of distant splicing events. Nat. Biotechnol. *33*, 736–742.
72. Childs, B.G., Durik, M., Baker, D.J., and van Deursen, J.M. (2015). Cellular senescence in aging and age-related disease: from mechanisms to therapy. Nat. Med. *21*, 1424–1435.
73. Vermeulen, M., Mulder, K.W., Denissov, S., Pijnappel, W.W.M.P., van Schaik, F.M.A., Varier, R.A., Baltissen, M.P.A., Stunnenberg, H.G., Mann, M., and Timmers, H.T.M. (2007). Selective anchoring of TFIID to nucleosomes by trimethylation of histone H3 lysine 4. Cell *131*, 58–69.
74. Yang, G., Zhang, L., Liu, W., Qiao, Z., Shen, S., Zhu, Q., Gao, R., Wang, M., Wang, M., Li, C., et al. (2021). Dux-mediated corrections of aberrant H3K9ac during 2-cell genome activation optimize efficiency of somatic cell nuclear transfer. Cell Stem Cell *28*, 150–163.e5.
75. Chen, T., and Dent, S.Y.R. (2014). Chromatin modifiers and remodellers: regulators of cellular differentiation. Nat. Rev. Genet. *15*, 93–106.
76. Klemm, S.L., Shipony, Z., and Greenleaf, W.J. (2019). Chromatin accessibility and the regulatory epigenome. Nat. Rev. Genet. *20*, 207–220.
77. Bates, S.E. (2020). Epigenetic therapies for cancer. N. Engl. J. Med. *383*, 650–663.
78. Cavalli, G., and Heard, E. (2019). Advances in epigenetics link genetics to the environment and disease. Nature *571*, 489–499.